Computers and Structures 161 (2015) 1–16

Contents lists available at ScienceDirect

Computers and Structures

journal homepage: www.elsevier.com/locate/compstruc

Formulation of the boundary element method in the wavenumber–frequency domain based on the thin layer method

João Manuel de Oliveira Barbosa [a,*], Eduardo Kausel [b], Álvaro Azevedo [a], Rui Calçada [a]

[a] Faculdade de Engenharia da Universidade do Porto, Rua Dr. Roberto Frias, s/n, 4200-465 Porto, Portugal
[b] Massachusetts Institute of Technology, 77 Massachusetts Avenue, Cambridge, MA 02139-4307, USA

ARTICLE INFO

Article history:
Received 9 May 2015
Accepted 13 August 2015

Keywords:
Boundary element method
Thin-layer method
Soil-structure
Invariant structures

ABSTRACT

This paper links the boundary element method (BEM) and the thin-layer method (TLM) in the context of structures that are invariant in one direction and for which the equations of motion can be formulated in the wavenumber–frequency domain (2.5D domain). The proposed combination differs from previous formulations in that one of the inverse Fourier transforms and the Green's functions (GF) integrals are obtained in closed form. This strategy is not only supremely efficient, but also avoids singularities when the collocation point belongs to the integrating boundary element, and provides accurate evaluations of the coefficients of the boundary element matrices.

1. Introduction

It is often the case that a domain can be idealized as a longitudinally invariant medium, i.e., a structure whose cross section remains constant along a given direction, say in direction y. For instance, in the case of vibrations induced by moving vehicles, it is often convenient to idealize the road, track or tunnel as a structure whose geometry is invariant in the longitudinal direction [1]. In that case, after carrying out a Fourier transform from the Cartesian spatial coordinate y to the horizontal wavenumber k_y, the analysis of the three dimensional structure can be reduced to a series of 2D problems. This type of analysis is referred to as a two-and-a-half dimensional (2.5D) problem and is normally cast in the wavenumber–frequency domain (k_y, ω).

Furthermore, whenever the domain under consideration is unbounded (e.g., soil-structure interaction problems), the radiation of waves at infinity must be accounted for. The boundary element method (BEM) intrinsically accounts for the radiation condition and therefore is one of the tools most commonly used in these situations. The BEM requires the availability of the so called fundamental solution (or Green's functions – GF), which in the vast majority of cases are those for a homogeneous, complete space (i.e. the Stokes–Kelvin problem), and rarely those of layered spaces. The reason for this is that in the 2.5D domain, the GF for homogeneous whole-spaces are known in analytical form [2], while the GF for layered spaces can only be obtained via numerical methods such as transfer matrices [3,4], stiffness matrices [5], or the thin-layer method (TLM) [6].

Formulations for the 2.5D BEM were previously given in Refs. [7,8] using the whole-space GF and in Ref. [9] using the GF for layered spaces obtained via the stiffness matrix method. In this work, we present a very efficient alternative formulation based on the Green's functions obtained with the TLM (2.5D BEM + TLM). When compared with the formulations in [7,8], the proposed procedure has the enormous advantage of avoiding the discretization of the free-surface of a half-space and of the interfaces between material layers, because layering is considered automatically in the definition of the GF. It accomplishes this at the expense of more elaborate computations to obtain the GF. When compared with the work presented in [9], the 2.5D BEM + TLM approach described herein replaces the discrete numerical Fourier inversion in k_y by exact modal summations, which requires solving a narrowly-banded quadratic eigenvalue problem. This circumvents the need for an appropriate wavenumber step for k_x and thus avoids the problems of spatial periodicity, wrap-around and aliasing. Another advantage of the 2.5D BEM + TLM is the avoidance of the numerical integration of the Green's functions over the boundary elements, which is replaced by modal summations, a feature that circumvents the complication entailed by the singularities contained in the GF.

This article is organized as follows: in Section 2 the TLM is reviewed and the expressions for the calculation of the 2.5D displacements and stresses are obtained; in Section 3 the direct calculation of the coefficients of the boundary element matrices

* Corresponding author.
E-mail address: dec08006@fe.up.pt (J.M. de Oliveira Barbosa).

http://dx.doi.org/10.1016/j.compstruc.2015.08.012
0045-7949/

is addressed; finally, in Section 4 the proposed procedure is validated by means of some examples.

2. TLM in the 2.5D domain – Green's functions

The TLM is an efficient semi-analytical method for the calculation of the fundamental solutions (i.e., GF) of layered media. It consists in expressing the displacement field in terms of a finite element expansion in the direction of layering together with analytical descriptions for the remaining directions. Though initially it was limited to domains of finite depth, paraxial boundaries were developed and coupled to the TLM in order to circumvent this limitation [10]. More recently, perfectly matched layers (PML) have been proposed and shown to be more accurate than paraxial boundaries for the simulation of unbounded domains [11].

The TLM has been formulated in the space-frequency domain (2D, 3D) [12] and in the wavenumber-time domain [13]. It has also been formulated in the 2.5D domain (x, k_y, ω) [14], but solely in terms of displacements elicited by applied forces, and has been coupled to the BEM in the context of 3D axisymmetric structures [15]. This section presents the derivation of the expressions for the displacements, their spatial derivatives and the stresses anywhere, both in the wavenumber domain (k_x, k_y, ω) and in the 2.5D domain (x, k_y, ω). Variables with an over-bar or tilde represent field quantities in the (k_x, k_y, ω) domain, while variables denoted without diacritical marks represent fields in the mixed (x, k_y, ω) domain.

2.1. Displacements in the wavenumber domain (k_x, k_y, ω)

In [14], a TLM formulation is presented in which the displacements elicited by various kinds of loads acting within layered media are obtained in the (k_x, k_y, ω) and (x, k_y, ω) domains. Following that work, after discretizing a layered domain into thin-layers and applying the principle of weighted residuals, we obtain a matrix equation for each thin-layer of the form

$$\overline{\mathbf{P}} = \left[k_x^2\mathbf{A}_{xx} + k_xk_y\mathbf{A}_{xy} + k_y^2\mathbf{A}_{yy} + i\left(k_x\mathbf{B}_x + k_y\mathbf{B}_y\right) + \left(\mathbf{G} - \omega^2\mathbf{M}\right)\right]\overline{\mathbf{U}} \quad (1)$$

where the vectors $\overline{\mathbf{P}}$ and $\overline{\mathbf{U}}$ contain, respectively, the external tractions $\overline{p}_\alpha(k_x, k_y, \omega)$ and displacements $\overline{u}_\alpha(k_x, k_y, \omega)$ at the nodal interfaces, and where the remaining boldface variables are matrices that depend solely on the material properties of the thin-layers. These matrices are listed in Appendix A for the case of cross-anisotropic materials. The variables k_x and k_y represent the horizontal wavenumbers in the transverse and longitudinal directions, respectively, ω represents the angular frequency, the index $\alpha(= x, y, z)$ represents the direction of the nodal displacement and/or traction, and $i = \sqrt{-1}$ is the imaginary unit.

By means of a similarity transformation, Eq. (1) can be changed into

$$\tilde{\mathbf{p}} = \left[k_x^2\mathbf{A}_{xx} + k_xk_y\mathbf{A}_{xy} + k_y^2\mathbf{A}_{yy} + k_x\tilde{\mathbf{B}}_x + k_y\tilde{\mathbf{B}}_y + \left(\mathbf{G} - \omega^2\mathbf{M}\right)\right]\tilde{\mathbf{u}} \quad (2)$$

where $\tilde{\mathbf{p}}$ and $\tilde{\mathbf{u}}$ are obtained from $\overline{\mathbf{P}}$ and $\overline{\mathbf{U}}$ by multiplying every third row by $-i$ and where $\tilde{\mathbf{B}}_x$ and $\tilde{\mathbf{B}}_y$ are obtained from $\mathbf{B}_x$ and $\mathbf{B}_y$ by simply reversing the sign of every third column. Eq. (2) is advantageous over Eq. (1) because the matrices therein are symmetric while in Eq. (1) they are not.

After assembling the thin-layer matrices for all the thin-layers, we obtain the global system of equations with the same configuration as Eq. (2), and although it can easily be solved for $\tilde{\mathbf{u}}$, we choose to follow an alternative and more convenient approach. In fact, the direct numerical solution of Eq. (2) for $\tilde{\mathbf{u}}$ (or $\tilde{\mathbf{p}}$) precludes the analytical evaluation of the inverse Fourier transforms from the (k_x, k_y, ω) domain to the (x, k_y, ω) domain, and consequently renders the TLM an inefficient method when compared with the stiffness matrix approach. For this reason, an alternative approach is followed wherein we find a modal basis with which we can calculate $\tilde{\mathbf{u}}$ and/or $\tilde{\mathbf{p}}$ through modal superposition. This procedure enables the analytical transformation of $\tilde{\mathbf{u}}$ and $\tilde{\mathbf{p}}$ to the desired 2.5D domain, which constitutes an enormous advantage.

Without entering into lengthy details, the modal basis is found by solving a quadratic eigenvalue problem in k of the form [14]

$$\left[k^2\mathbf{A}_{xx} + k\tilde{\mathbf{B}}_x + \left(\mathbf{G} - \omega^2\mathbf{M}\right)\right]\boldsymbol{\phi} = \mathbf{0} \quad (3)$$

Rearranging the matrices in this eigenvalue problem by degrees of freedom (first x, then y and finally z), we observe that these matrices attain the following structures

$$\mathbf{A}_{xx} = \begin{bmatrix} \mathbf{A}_x & \mathbf{0} & \mathbf{0} \\ \mathbf{0} & \mathbf{A}_y & \mathbf{0} \\ \mathbf{0} & \mathbf{0} & \mathbf{A}_z \end{bmatrix} \qquad \tilde{\mathbf{B}}_x = \begin{bmatrix} \mathbf{0} & \mathbf{0} & \mathbf{B}_{xz} \\ \mathbf{0} & \mathbf{0} & \mathbf{0} \\ \mathbf{B}_{xz}^T & \mathbf{0} & \mathbf{0} \end{bmatrix}$$
$$\mathbf{G} = \begin{bmatrix} \mathbf{G}_x & \mathbf{0} & \mathbf{0} \\ \mathbf{0} & \mathbf{G}_y & \mathbf{0} \\ \mathbf{0} & \mathbf{0} & \mathbf{G}_z \end{bmatrix} \qquad \mathbf{M} = \begin{bmatrix} \mathbf{M}_x & \mathbf{0} & \mathbf{0} \\ \mathbf{0} & \mathbf{M}_y & \mathbf{0} \\ \mathbf{0} & \mathbf{0} & \mathbf{M}_z \end{bmatrix} \quad (4)$$

Because of the special structure of these matrices, the eigenvalue problem in Eq. (3) can be decoupled into the following two eigenvalue problems

$$\left\{k^2\begin{bmatrix} \mathbf{A}_x & \mathbf{0} \\ \mathbf{0} & \mathbf{A}_z \end{bmatrix} + k\begin{bmatrix} \mathbf{0} & \mathbf{B}_{xz} \\ \mathbf{B}_{xz}^T & \mathbf{0} \end{bmatrix} + \begin{bmatrix} \mathbf{C}_x & \mathbf{0} \\ \mathbf{0} & \mathbf{C}_z \end{bmatrix}\right\}\begin{bmatrix} \boldsymbol{\phi}_x \\ \boldsymbol{\phi}_z \end{bmatrix} = \begin{bmatrix} \mathbf{0} \\ \mathbf{0} \end{bmatrix}$$
$$\left(k^2\mathbf{A}_y + \mathbf{C}_y\right)\boldsymbol{\phi}_y = \mathbf{0} \quad (5)$$

which correspond to the generalized Rayleigh and generalized Love eigenvalue problems. The first eigenvalue problem has $2N_R$ solutions while the second has $2N_L$ solutions, with N_R and N_L being the dimension of the corresponding matrices. For the calculation of the responses, only the solutions that correspond to eigenvalues with negative imaginary components are considered, because only these entail waves that carry energy away from the source. Hence only N_R solutions of the Rayleigh problem and only N_L solutions of the Love problem are considered. Based on the eigensolutions, the displacements $\overline{u}_{\alpha\beta}^{(mn)}$ at the mth nodal interface in direction α due to a unit load applied at the nth nodal interface in direction β are calculated by modal superposition as listed in Table 1, with the coefficients K_{ij} given in Table 2.

The displacements at an interior horizontal plane of the ith thin-layer are obtained by vertical interpolation of the nodal values, i.e.,

$$\overline{u}_{\alpha\beta}(z) = \sum_{j=1}^{nn} N_j(z)\overline{u}_{\alpha\beta(j)}^{(i)} \quad (6)$$

with nn being the number of nodal interfaces within each thin-layer ($nn = 2$ for linear expansion, $nn = 3$ for quadratic expansion, etc.), $\overline{u}_{\alpha\beta(j)}^{(i)}$ the nodal displacement of the jth nodal interface of the considered thin-layer, and $N_j(z)$ the corresponding shape function.

Table 1
Nodal displacements in frequency–wavenumber domain.

$\overline{u}_{xx}^{(mn)} = \sum_j^{N_R} K_{3j}\,\phi_{xj}^{(m)}\,\phi_{xj}^{(n)} + \sum_j^{N_L} K_{4j}\phi_{yj}^{(m)}\,\phi_{yj}^{(n)}$	
$\overline{u}_{yy}^{(mn)} = \sum_j^{N_R} K_{4j}\,\phi_{xj}^{(m)}\,\phi_{xj}^{(n)} + \sum_j^{N_L} K_{3j}\,\phi_{yj}^{(m)}\,\phi_{yj}^{(n)}$	
$\overline{u}_{xy}^{(mn)} = \sum_j^{N_R} K_{2j}\,\phi_{xj}^{(m)}\,\phi_{xj}^{(n)} - \sum_j^{N_L} K_{2j}\,\phi_{yj}^{(m)}\,\phi_{yj}^{(n)} = \overline{u}_{yx}^{(mn)}$	
$\overline{u}_{xz}^{(mn)} = -i\sum_j^{N_R} K_{5j}\,\phi_{xj}^{(m)}\,\phi_{zj}^{(n)}$	$\overline{u}_{zx}^{(mn)} = i\sum_j^{N_R} K_{5j}\,\phi_{zj}^{(m)}\,\phi_{xj}^{(n)} = -\overline{u}_{xz}^{(nm)}$
$\overline{u}_{yz}^{(mn)} = -i\sum_j^{N_R} K_{6j}\,\phi_{xj}^{(m)}\,\phi_{zj}^{(n)}$	$\overline{u}_{zy}^{(mn)} = i\sum_{j=1}^{N_R} K_{6j}\,\phi_{zj}^{(m)}\,\phi_{xj}^{(n)} = -\overline{u}_{yz}^{(nm)}$
$\overline{u}_{zz}^{(mn)} = \sum_j^{N_R} K_{1j}\,\phi_{zj}^{(m)}\,\phi_{zj}^{(n)}$	

2.2. Consistent nodal tractions in the wavenumber domain (k_x, k_y, ω)

The consistent nodal tractions acting on one isolated thin-layer (say the ith thin-layer, limited by the nodal interfaces l and m, Fig. 1) are obtained through Eq. (2), but with $\tilde{\mathbf{p}}$ and $\tilde{\mathbf{u}}$ representing the collection of nodal tractions and displacements of the single, free thin-layer. Thus, assuming an external force in direction β, the vectors $\tilde{\mathbf{p}}$ and $\tilde{\mathbf{u}}$ are

$$\tilde{\mathbf{p}}^{(i)} = \begin{bmatrix} \tilde{\mathbf{p}}^{(i)}_{(1)} \\ \vdots \\ \tilde{\mathbf{p}}^{(i)}_{(nn+1)} \end{bmatrix} \quad \tilde{\mathbf{u}}^{(i)} = \begin{bmatrix} \tilde{\mathbf{u}}^{(i)}_{(1)} \\ \vdots \\ \tilde{\mathbf{u}}^{(i)}_{(nn+1)} \end{bmatrix} \tag{7}$$

with $\tilde{\mathbf{p}}^{(i)}_{(k)} = \left\{ \overline{p}^{(i)}_{x\beta(k)} \quad \overline{p}^{(i)}_{y\beta(k)} \quad -i\overline{p}^{(i)}_{z\beta(k)} \right\}^{\mathrm{T}}$ being the modified nodal tractions and $\tilde{\mathbf{u}}^{(i)}_{(k)} = \left\{ \overline{u}^{(i)}_{x\beta(k)} \quad \overline{u}^{(i)}_{y\beta(k)} \quad -i\overline{u}^{(i)}_{z\beta(k)} \right\}^{\mathrm{T}}$ being the modified nodal displacements (the word "modified" refers to the multiplication by $-i$).

In the ensuing and for the sake of simplicity, it will be assumed that no external forces act at internal (i.e. intermediate) interfaces, which exist when $nn > 2$. Thus, the only non-zero components of the traction vector $\tilde{\mathbf{p}}$ are $\overline{p}^{(i)}_{\alpha\beta(1)}$ and $\overline{p}^{(i)}_{\alpha\beta\ (nn)}$. These components correspond to the tractions that the remaining part of the domain transmits to the current thin-layer through its upper and lower interfaces.

After replacing in Eq. (2) the displacements by their modal expansion as given in Table 1, we obtain the consistent tractions expressed also in terms of a modal superposition. Hence, considering first a force in direction $\beta = x$ applied at the global interface n, the nodal tractions at the ith thin-layer are obtained with

$$\begin{aligned}
\tilde{\mathbf{p}}^{(i)} = \mathbf{A}_{xx} \Bigg(& \sum_{j=1}^{N_R} \phi^{(n)}_{xj} \begin{bmatrix} \Gamma^{(x2)}_{jR} & & \\ & \ddots & \\ & & \Gamma^{(x2)}_{jR} \end{bmatrix} \begin{bmatrix} \mathbf{\Phi}^{(l)}_{Rj} \\ \vdots \\ \mathbf{\Phi}^{(m)}_{Rj} \end{bmatrix} + \sum_{j=1}^{N_L} \phi^{(n)}_{yj} \begin{bmatrix} \Gamma^{(x2)}_{jL} & & \\ & \ddots & \\ & & \Gamma^{(x2)}_{jL} \end{bmatrix} \begin{bmatrix} \mathbf{\Phi}^{(l)}_{Lj} \\ \vdots \\ \mathbf{\Phi}^{(m)}_{Lj} \end{bmatrix} \Bigg) \\
& + \left(k_y \mathbf{A}_{xy} + \tilde{\mathbf{B}}_x\right) \Bigg(\sum_{j=1}^{N_R} \phi^{(n)}_{xj} \begin{bmatrix} \Gamma^{(x1)}_{jR} & & \\ & \ddots & \\ & & \Gamma^{(x1)}_{jR} \end{bmatrix} \begin{bmatrix} \mathbf{\Phi}^{(l)}_{Rj} \\ \vdots \\ \mathbf{\Phi}^{(m)}_{Rj} \end{bmatrix} + \sum_{j=1}^{N_L} \phi^{(n)}_{yj} \begin{bmatrix} \Gamma^{(x1)}_{jL} & & \\ & \ddots & \\ & & \Gamma^{(x1)}_{jL} \end{bmatrix} \begin{bmatrix} \mathbf{\Phi}^{(l)}_{Lj} \\ \vdots \\ \mathbf{\Phi}^{(m)}_{Lj} \end{bmatrix} \Bigg) \\
& + \left(k_y^2 \mathbf{A}_{yy} + k_y \tilde{\mathbf{B}}_y + \mathbf{G} - \omega^2 \mathbf{M}\right) \Bigg(\sum_{j=1}^{N_R} \phi^{(n)}_{xj} \begin{bmatrix} \Gamma^{(x0)}_{jR} & & \\ & \ddots & \\ & & \Gamma^{(x0)}_{jR} \end{bmatrix} \begin{bmatrix} \mathbf{\Phi}^{(l)}_{Rj} \\ \vdots \\ \mathbf{\Phi}^{(m)}_{Rj} \end{bmatrix} + \sum_{j=1}^{N_L} \phi^{(n)}_{yj} \begin{bmatrix} \Gamma^{(x0)}_{jL} & & \\ & \ddots & \\ & & \Gamma^{(x0)}_{jL} \end{bmatrix} \begin{bmatrix} \mathbf{\Phi}^{(l)}_{Lj} \\ \vdots \\ \mathbf{\Phi}^{(m)}_{Lj} \end{bmatrix} \Bigg)
\end{aligned} \tag{8}$$

where

$$\Gamma^{(xp)}_{jR} = \begin{bmatrix} k_x^p K_{3j}(k_x, k_y) & 0 & 0 \\ 0 & k_x^p K_{2j}(k_x, k_y) & 0 \\ 0 & 0 & k_x^p K_{5j}(k_x, k_y) \end{bmatrix} \tag{9}$$

Table 2
Kernels K_{ij}.

$K_{1j} = \frac{1}{k^2 - k_j^2}$	$K_{2j} = \frac{k_x k_y}{k^2 (k^2 - k_j^2)}$
$K_{3j} = \frac{k_x^2}{k^2 (k^2 - k_j^2)}$	$K_{4j} = \frac{k_y^2}{k^2 (k^2 - k_j^2)}$
$K_{5j} = \frac{k_x}{k_j (k^2 - k_j^2)}$	$K_{6j} = \frac{k_y}{k_j (k^2 - k_j^2)}$

$$\Gamma^{(xp)}_{jL} = \begin{bmatrix} k_x^p K_{4j}(k_x, k_y) & 0 & 0 \\ 0 & -k_x^p K_{2j}(k_x, k_y) & 0 \\ 0 & 0 & 0 \end{bmatrix} \tag{10}$$

$$\mathbf{\Phi}^{(k)}_{Rj} = \left\{ \phi^{(k)}_{xj} \quad \phi^{(k)}_{xj} \quad \phi^{(k)}_{zj} \right\}^{\mathrm{T}} \quad \mathbf{\Phi}^{(k)}_{Lj} = \left\{ \phi^{(k)}_{yj} \quad \phi^{(k)}_{yj} \quad 0 \right\}^{\mathrm{T}} \quad k = l \ldots m \tag{11}$$

Similarly, for a load in direction $\beta = y$, the consistent nodal tractions are calculated as

$$\begin{aligned}
\tilde{\mathbf{p}}^{(i)} = \mathbf{A}_{xx} \Bigg(& \sum_{j=1}^{N_R} \phi^{(n)}_{xj} \begin{bmatrix} \Gamma^{(y2)}_{jR} & & \\ & \ddots & \\ & & \Gamma^{(y2)}_{jR} \end{bmatrix} \begin{bmatrix} \mathbf{\Phi}^{(l)}_{Rj} \\ \vdots \\ \mathbf{\Phi}^{(m)}_{Rj} \end{bmatrix} + \sum_{j=1}^{N_L} \phi^{(n)}_{yj} \begin{bmatrix} \Gamma^{(y2)}_{jL} & & \\ & \ddots & \\ & & \Gamma^{(y2)}_{jL} \end{bmatrix} \begin{bmatrix} \mathbf{\Phi}^{(l)}_{Lj} \\ \vdots \\ \mathbf{\Phi}^{(m)}_{Lj} \end{bmatrix} \Bigg) \\
& + \left(k_y \mathbf{A}_{xy} + \tilde{\mathbf{B}}_x\right) \Bigg(\sum_{j=1}^{N_R} \phi^{(n)}_{xj} \begin{bmatrix} \Gamma^{(y1)}_{jR} & & \\ & \ddots & \\ & & \Gamma^{(y1)}_{jR} \end{bmatrix} \begin{bmatrix} \mathbf{\Phi}^{(l)}_{Rj} \\ \vdots \\ \mathbf{\Phi}^{(m)}_{Rj} \end{bmatrix} + \sum_{j=1}^{N_L} \phi^{(n)}_{yj} \begin{bmatrix} \Gamma^{(y1)}_{jL} & & \\ & \ddots & \\ & & \Gamma^{(y1)}_{jL} \end{bmatrix} \begin{bmatrix} \mathbf{\Phi}^{(l)}_{Lj} \\ \vdots \\ \mathbf{\Phi}^{(m)}_{Lj} \end{bmatrix} \Bigg) \\
& + \left(k_y^2 \mathbf{A}_{yy} + k_y \tilde{\mathbf{B}}_y + \mathbf{G} - \omega^2 \mathbf{M}\right) \Bigg(\sum_{j=1}^{N_R} \phi^{(n)}_{xj} \begin{bmatrix} \Gamma^{(y0)}_{jR} & & \\ & \ddots & \\ & & \Gamma^{(y0)}_{jR} \end{bmatrix} \begin{bmatrix} \mathbf{\Phi}^{(l)}_{Rj} \\ \vdots \\ \mathbf{\Phi}^{(m)}_{Rj} \end{bmatrix} + \sum_{j=1}^{N_L} \phi^{(n)}_{yj} \begin{bmatrix} \Gamma^{(y0)}_{jL} & & \\ & \ddots & \\ & & \Gamma^{(y0)}_{jL} \end{bmatrix} \begin{bmatrix} \mathbf{\Phi}^{(l)}_{Lj} \\ \vdots \\ \mathbf{\Phi}^{(m)}_{Lj} \end{bmatrix} \Bigg)
\end{aligned} \tag{12}$$

with

$$\Gamma^{(yp)}_{jR} = \begin{bmatrix} k_x^p K_{2j}(k_x, k_y) & 0 & 0 \\ 0 & k_x^p K_{4j}(k_x, k_y) & 0 \\ 0 & 0 & k_x^p K_{6j}(k_x, k_y) \end{bmatrix} \tag{13}$$

$$\Gamma^{(yp)}_{jL} = \begin{bmatrix} -k_x^p K_{2j}(k_x, k_y) & 0 & 0 \\ 0 & k_x^p K_{3j}(k_x, k_y) & 0 \\ 0 & 0 & 0 \end{bmatrix} \tag{14}$$

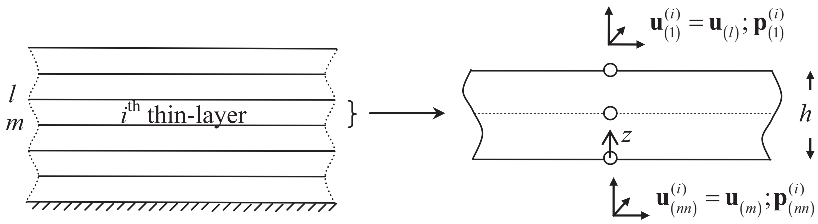

Fig. 1. Stack of thin-layers (on the left) and single thin-layer detail (on the right).

Finally, for a load in the direction $\beta = z$, the tractions are calculated as

$$\begin{aligned}\tilde{\mathbf{p}}^{(i)} = \mathbf{A}_{xx}&\left(\sum_{j=1}^{N_R}\phi_{zj}^{(n)}\begin{bmatrix}\Gamma_{jR}^{(z2)} & & \\ & \ddots & \\ & & \Gamma_{jR}^{(z2)}\end{bmatrix}\begin{bmatrix}\mathbf{\Phi}_{Rj}^{(l)}\\ \vdots \\ \mathbf{\Phi}_{Rj}^{(m)}\end{bmatrix}\right)\\ &+\left(k_y\mathbf{A}_{xy}+\tilde{\mathbf{B}}_x\right)\left(\sum_{j=1}^{N_R}\phi_{zj}^{(n)}\begin{bmatrix}\Gamma_{jR}^{(z1)} & & \\ & \ddots & \\ & & \Gamma_{jR}^{(z1)}\end{bmatrix}\begin{bmatrix}\mathbf{\Phi}_{Rj}^{(l)}\\ \vdots \\ \mathbf{\Phi}_{Rj}^{(m)}\end{bmatrix}\right)\\ &+\left(k_y^2\mathbf{A}_{yy}+k_y\tilde{\mathbf{B}}_y+\mathbf{G}-\omega^2\mathbf{M}\right)\left(\sum_{j=1}^{N_R}\phi_{zj}^{(n)}\begin{bmatrix}\Gamma_{jR}^{(z0)} & & \\ & \ddots & \\ & & \Gamma_{jR}^{(z0)}\end{bmatrix}\begin{bmatrix}\mathbf{\Phi}_{Rj}^{(l)}\\ \vdots \\ \mathbf{\Phi}_{Rj}^{(m)}\end{bmatrix}\right)\end{aligned} \tag{15}$$

with

$$\Gamma_{jR}^{(zp)} = -i\begin{bmatrix}k_x^pK_{5j}(k_x,k_y) & 0 & 0\\ 0 & k_x^pK_{6j}(k_x,k_y) & 0\\ 0 & 0 & k_x^pK_{1j}(k_x,k_y)\end{bmatrix} \tag{16}$$

2.3. Vertical derivatives and internal stresses in the wavenumber domain (k_x, k_y, ω)

In the (k_x, k_y, ω) domain, the derivatives of the displacements along the two horizontal directions x and y (herein termed horizontal derivatives) are obtained simply by multiplying the displacements by $-ik_x$ or $-ik_y$, depending on the direction x or y of the derivatives. As for the derivatives along the vertical direction z (herein termed vertical derivatives, with z pointing upwards), they can be obtained by combining the nodal displacements weighted by the derivatives of the associated shape functions. However, since the displacement field in the vertical direction is discrete, that procedure yields derivatives at the top and bottom interfaces of the thin-layers that are not consistent with the nodal tractions derived in Section 2.2, and therefore their degree of accuracy is inferior.

In [16], an alternative procedure for the calculation of the derivatives is proposed that allows computing stresses with the same degree of accuracy as the displacements. This procedure is based on the definition of secondary interpolation functions that are consistent with the stresses at the top and bottom interfaces of the thin-layer. Herein, that same procedure is used to define the vertical derivatives and subsequently the internal stresses at the internal nodal interfaces.

Assume for now that the following quantities are already known: displacements $\overline{u}^{(i)}_{\alpha\beta(j)}$ at the $j = 1, \ldots, nn+1$ nodal interfaces of the ith thin-layer, and their horizontal derivatives $\overline{u}^{(i)}_{\alpha\beta,x(j)}$ and $\overline{u}^{(i)}_{\alpha\beta,y(j)}$; consistent tractions $\overline{p}^{(i)}_{\alpha\beta(1)}$ and $\overline{p}^{(i)}_{\alpha\beta\,(nn)}$ at the top and bottom nodal interfaces (α is the direction of the response and β is the direction of the force). The tractions at the upper surface relate to the internal stresses through

$$\tilde{\mathbf{p}}^{(i)}_{(1)} = \left\{\,\overline{\tau}^{\text{top}}_{xz\beta} \quad \overline{\tau}^{\text{top}}_{yz\beta} \quad -i\overline{\sigma}^{\text{top}}_{zz\beta}\,\right\}^{\mathrm{T}} \tag{17}$$

and the tractions at the lower surface relate to the internal stresses through

$$\tilde{\mathbf{p}}^{(i)}_{(nn)} = -\left\{\,\overline{\tau}^{\text{bottom}}_{xz\beta} \quad \overline{\tau}^{\text{bottom}}_{yz\beta} \quad -i\overline{\sigma}^{\text{bottom}}_{zz\beta}\,\right\}^{\mathrm{T}} \tag{18}$$

Additionally, the internal stresses relate to the derivatives of displacements through

$$\begin{cases}\overline{\tau}_{xz\beta} = G\left(\overline{u}_{x\beta,z}+\overline{u}_{z\beta,x}\right)\\ \overline{\tau}_{yz\beta} = G\left(\overline{u}_{y\beta,z}+\overline{u}_{z\beta,y}\right)\\ \overline{\sigma}_{zz\beta} = \lambda\left(\overline{u}_{x\beta,x}+\overline{u}_{y\beta,y}\right)+(\lambda+2G)\overline{u}_{z\beta,z}\end{cases} \tag{19}$$

where G and λ are the Lamé constants. Eq. (19) can be solved for the vertical derivatives, yielding

$$\begin{cases}\overline{u}_{x\beta,z} = \frac{\left(\tau_{xz\beta}-G\overline{u}_{z\beta,x}\right)}{G}\\ \overline{u}_{y\beta,z} = \frac{\left(\tau_{yz\beta}-G\overline{u}_{z\beta,y}\right)}{G}\\ \overline{u}_{z\beta,z} = \frac{\sigma_{zz\beta}-\lambda\left(\overline{u}_{x\beta,x}+\overline{u}_{y\beta,y}\right)}{(\lambda+2G)}\end{cases} \tag{20}$$

We now have expressions for the displacements at each of the nn nodal interfaces and for their vertical derivatives at the upper and lower interfaces. With the $nn+2$ known variables, we can use Hermitian interpolation to find a polynomial of degree $nn+1$ that closely approximates the variation of displacements with the vertical coordinate. For example, if we assume that the thin-layer is of quadratic expansion $(nn = 3)$ and that its thickness is h, then

$$\overline{u}_{\alpha\beta}(z) = A_{\alpha\beta}+B_{\alpha\beta}z+C_{\alpha\beta}z^2+D_{\alpha\beta}z^3+E_{\alpha\beta}z^4 \tag{21}$$

$$\overline{u}_{\alpha\beta,z}(z) = B_{\alpha\beta}+2C_{\alpha\beta}z+3D_{\alpha\beta}z^2+4E_{\alpha\beta}z^3 \tag{22}$$

$$\begin{bmatrix}A_{\alpha\beta}\\ B_{\alpha\beta}\\ C_{\alpha\beta}\\ D_{\alpha\beta}\\ E_{\alpha\beta}\end{bmatrix} = \begin{bmatrix}1 & 0 & 0 & 0 & 0\\ 1 & h/2 & (h/2)^2 & (h/2)^3 & (h/2)^4\\ 1 & h & h^2 & h^3 & h^4\\ 0 & 1 & 0 & 0 & 0\\ 0 & 1 & 2h & 3h^2 & 4h^3\end{bmatrix}^{-1}\begin{bmatrix}\overline{u}^{(i)}_{\alpha\beta(3)}\\ \overline{u}^{(i)}_{\alpha\beta(2)}\\ \overline{u}^{(i)}_{\alpha\beta(1)}\\ \overline{u}^{(i)}_{\alpha\beta,z(3)}\\ \overline{u}^{(i)}_{\alpha\beta,z(1)}\end{bmatrix} \tag{23}$$

After obtaining the left-hand side of Eq. (23), the vertical derivatives of the displacements at the nodal interfaces can be determined with Eq. (22). With the horizontal and vertical derivatives known, the internal stresses at all nodal interfaces are obtained through Eq. (19).

The stresses $\overline{\sigma}_{\alpha z\beta}(z)$ and the vertical derivatives $\overline{u}_{\alpha\beta,z}(z)$ inside the thin-layer can be calculated using Eq. (22) and then Eq. (19). Nonetheless, we choose to use the original shape functions to interpolate these variables, i.e.,

$$\overline{u}_{\alpha\beta,z}(z)=\sum_{j=1}^{nn}N_j(z)\overline{u}^{(i)}_{\alpha\beta,z(j)} \tag{24}$$

$$\overline{\sigma}_{\alpha z\beta}(z)=\sum_{j=1}^{nn}N_j(z)\overline{\sigma}^{(i)}_{\alpha z\beta(j)} \tag{25}$$

2.4. Variable fields in the 2.5D domain (x, k_y, ω)

Ultimately, in the context of the 2.5D BEM, the variable fields needed must be expressed in the (x, k_y, ω) domain, which is attained by means of the inverse Fourier transform

$$f(x,k_y,\omega)=\frac{1}{2\pi}\int_{-\infty}^{+\infty}\bar{f}(k_x,k_y,\omega)e^{-ik_x x}dk_x \tag{26}$$

In Eq. (26), f represents either the displacements, their derivatives, the nodal tractions, or the internal stresses. Since these variables are all given explicitly in terms of the kernels K_{ij} defined in Table 2 (in some cases these kernels are multiplied by k_x or k_x^2), then the integral in Eq. (26) can be evaluated analytically by means of contour integration [17]. In the ensuing, the evaluation of the inverse Fourier transforms for the displacements, their derivatives, and tractions is addressed.

In the wavenumber domain (k_x, k_y, ω), the displacements are obtained as explained in Table 1. Their transformation to the space domain (x, k_y, ω), according to Eq. (26), requires the evaluation of the integrals

$$I^{(0)}_{ij}(x,k_y,\omega)=\frac{1}{2\pi}\int_{-\infty}^{+\infty}K_{ij}e^{-ik_x x}dk_x \tag{27}$$

Closed form expressions for these integrals are given in [14] and are reproduced in Appendix B. After determining $I^{(0)}_{ij}$, the displacements in $u^{(mn)}_{\alpha\beta}(x,k_y,\omega)$ are obtained by replacing in Table 1 K_{ij} by $I^{(0)}_{ij}$. For example, the displacements $u^{(mn)}_{xx}$ is calculated with

$$u^{(mn)}_{xx}=\sum_{j}^{N_R}I^{(0)}_{3j}\phi^{(m)}_{xj}\phi^{(n)}_{xj}+\sum_{j}^{N_L}I^{(0)}_{4j}\phi^{(m)}_{yj}\phi^{(n)}_{yj} \tag{28}$$

Concerning the derivatives in the y direction, they are obtained simply by multiplying the displacements $u^{(mn)}_{\alpha\beta}(x,k_y,\omega)$ by $-ik_y$. For instance, the derivative $u^{(mn)}_{xx,y}$ is calculated with

$$u^{(mn)}_{xx,y}=-ik_y u^{(mn)}_{xx} \tag{29}$$

In turn, the derivatives in the x direction require the evaluation of the integrals

$$I^{(1)}_{ij}(x,k_y,\omega)=\frac{1}{2\pi}\int_{-\infty}^{+\infty}k_xK_{ij}e^{-ik_x x}dk_x \tag{30}$$

whose closed form expressions are also listed in Appendix B. The x-derivatives are then obtained by replacing in Table 1 K_{ij} by $-iI^{(1)}_{ij}$. For example, the derivative $u^{(mn)}_{xx,x}$ is calculated with

$$u^{(mn)}_{xx,x}=-i\sum_{j}^{N_R}I^{(1)}_{3j}\phi^{(m)}_{xj}\phi^{(n)}_{xj}-i\sum_{j}^{N_L}I^{1}_{4j}\phi^{(m)}_{yj}\phi^{(n)}_{yj} \tag{31}$$

For the calculation of the consistent nodal tractions, besides $I^{(0)}_{ij}$ and $I^{(1)}_{ij}$, the integrals

$$I^{(2)}_{ij}(x,k_y,\omega)=\frac{1}{2\pi}\int_{-\infty}^{+\infty}k_x^2K_{ij}e^{-ik_x x}dk_x \tag{32}$$

are also needed, and are given in Appendix B. The nodal tractions are then obtained using Eqs. (8)–(16), but with the quantities $k_x^pK_{ij}$ in matrices $\Gamma^{(\beta p)}_{jR}$ replaced by the appropriate value of $I^{(p)}_{ij}$. For example, for a force in the direction $\beta = z$, Eq. (15) becomes

$$\begin{aligned}\mathbf{p}^{(i)}=\mathbf{A}_{xx}&\left(\sum_{j=1}^{N_R}\phi^{(n)}_{zj}\begin{bmatrix}\Lambda^{(z2)}_{jR}&&\\&\ddots&\\&&\Lambda^{(z2)}_{jR}\end{bmatrix}\begin{bmatrix}\boldsymbol{\Phi}^{(l)}_{Rj}\\ \vdots\\ \boldsymbol{\Phi}^{(m)}_{Rj}\end{bmatrix}\right)\\&+(k_y\mathbf{A}_{xy}+\mathbf{B}_x)\left(\sum_{j=1}^{N_R}\phi^{(n)}_{zj}\begin{bmatrix}\Lambda^{(z1)}_{jR}&&\\&\ddots&\\&&\Lambda^{(z1)}_{jR}\end{bmatrix}\begin{bmatrix}\boldsymbol{\Phi}^{(l)}_{Rj}\\ \vdots\\ \boldsymbol{\Phi}^{(m)}_{Rj}\end{bmatrix}\right)\\&+\left(k_y^2\mathbf{A}_{yy}+k_y\mathbf{B}_y+\mathbf{G}-\omega^2\mathbf{M}\right)\left(\sum_{j=1}^{N_R}\phi^{(n)}_{zj}\begin{bmatrix}\Lambda^{(z0)}_{jR}&&\\&\ddots&\\&&\Lambda^{(z0)}_{jR}\end{bmatrix}\begin{bmatrix}\boldsymbol{\Phi}^{(l)}_{Rj}\\ \vdots\\ \boldsymbol{\Phi}^{(m)}_{Rj}\end{bmatrix}\right)\end{aligned} \tag{33}$$

where

$$\Lambda^{(zp)}_{jR}=-i\begin{bmatrix}I^{(p)}_{5j}(x,k_y)&0&0\\0&I^{(p)}_{6j}(x,k_y)&0\\0&0&I^{(p)}_{1j}(x,k_y)\end{bmatrix} \tag{34}$$

The calculation of the vertical derivatives and of the internal stresses in the space domain follows along exactly the same steps given by Eqs. (20)–(25), provided that all variables in these expressions are known in the spatial domain. This is so because the operation for derivatives and stresses commutes with the Fourier inversion from the wavenumber domain into the space domain. The secondary interpolation functions must, therefore, be defined for each different combination of (x, k_y, ω).

3. Direct calculation of the BEM coefficients via the TLM

The integral representation theorem in the 2.5D domain states that [8]

$$\begin{aligned}\kappa u_\alpha(x_\xi,k_y,z_\xi,\omega)=&\sum_{\beta=x,y,z}\int_\Gamma u^*_{\beta\alpha}(x,z,x_\xi,z_\xi,-k_y,\omega)p^{\mathbf{n}}_\beta(x,k_y,z,\omega)d\Gamma\\&-\sum_{\beta=x,y,z}\int_\Gamma p^{\mathbf{n}*}_{\beta\alpha}(x,z,x_\xi,z_\xi,-k_y,\omega)u_\beta(x,k_y,z,\omega)d\Gamma\end{aligned} \tag{35}$$

where $\mathbf{x} = (x, z)$ is a general point that belongs to the boundary Γ of the domain Ω; $\mathbf{n}$ is the outward normal to this boundary; $\mathbf{x}_\xi = (x_\xi, z_\xi)$ is a collocation point; κ is 1 if $\mathbf{x}_\xi \in \Omega$ and 0 otherwise; α is the direction of the load applied at the collocation point; $u_\beta(\ldots)$ is the displacement field in direction β; $p^{\mathbf{n}}_\beta(\ldots)$ is the traction field in direction β, which is defined by

$$p^{\mathbf{n}}_\beta(\ldots)=\sum_{j=x,z}\sigma_{\beta j}(\ldots)n_j \tag{36}$$

with n_j being the components of the outwards normal $\mathbf{n}$ of the boundary; and where $u^*_{\beta\alpha}(\ldots)$ and $p^{\mathbf{n}*}_{\beta\alpha}(\ldots)$ are the Green's functions, i.e., the displacements and tractions in the direction β at the point $\mathbf{x}$ that belongs to an auxiliary domain (in this work, an horizontally layered domain) induced by an impulsive point load with direction α applied at the collocation point $\mathbf{x}_\xi$.

Since the GF present singularities at the collocation points, i.e., when $\mathbf{x} \to \mathbf{x}_\xi$, Eq. (35) must be regularized. One possible regularization procedure is to remove the collocation point $\mathbf{x}_\xi$ from the boundary by slightly modifying it [18]. For example, in Fig. 2

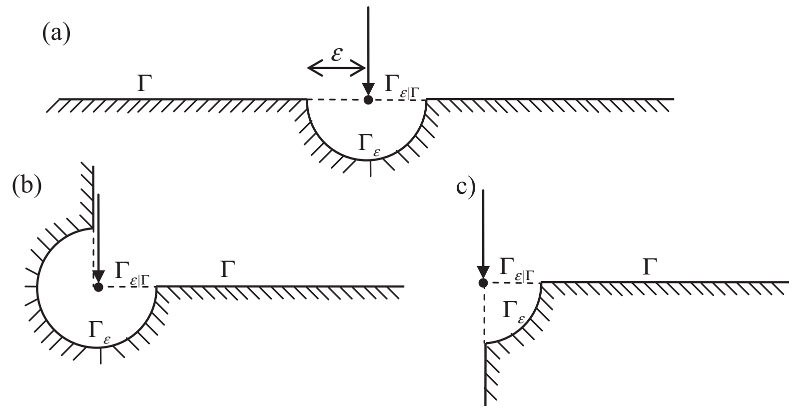

Fig. 2. Strategies for circumventing the collocation points. (a) Smooth horizontal boundary; (b) concave corner; (c) convex corner.

suggests possible alterations of the boundary that excludes the collocation point.

After the application of the regularization procedure, the boundary integral representation becomes [18]

$$\sum_{\beta=x,y,z} c_{\alpha\beta} u_\beta(x_\xi,k_y,z_\xi,\omega) = \sum_{\beta=x,y,z} \int_\Gamma u^*_{\beta\alpha}(x,z,x_\xi,z_\xi,-k_y,\omega) p^{\mathbf{n}}_\beta(x,k_y,z,\omega)\, d\Gamma - \sum_{\beta=x,y,z} \int_\Gamma p^{\mathbf{n}*}_{\beta\alpha}(x,z,x_\xi,z_\xi,-k_y,\omega) u_\beta(x,k_y,z,\omega)\, d\Gamma \tag{37}$$

where $c_{\alpha\beta}$ is a factor that depends on the geometry of the boundary at the collocation point $\mathbf{x}_\xi$ and on the type of auxiliary domain used for the calculation of the GF. If the GF used are those of a homogeneous whole-space and if the boundary is smooth at the collocation point (Fig. 2a), then $c_{\alpha\beta} = 0.5\delta_{\alpha\beta}$. This value is due to the symmetry of the GF for a homogeneous whole-space, a condition that holds true for any load direction. For different boundary geometries and while using GF for the homogeneous whole-space, Guiguiani [19] and Mantic [20] describe procedures for the calculation of the factor $c_{\alpha\beta}$. If the auxiliary domain used for the calculation of the GF is not homogeneous, then the identity $c_{\alpha\beta} = 0.5\delta_{\alpha\beta}$ for smooth boundaries and the procedures presented by Guiguiani and Mantic do not apply, and therefore different approaches for the calculation of $c_{\alpha\beta}$ must be considered.

The boundary element method results from the discretization of the boundary Γ in Eq. (37) and from the approximation of the displacement and traction fields at the boundary. Its application yields a system of equations of the form (see [18] for details),

$$(\mathbf{C} + \mathbf{Q})\mathbf{u} = \mathbf{H}\mathbf{p} \tag{38}$$

in which the matrix $\mathbf{C}$ is block-diagonal containing the factors $c_{\alpha\beta}$ of all of the collocation points, $\mathbf{Q}$ is a square matrix that collects the coefficients $Q_{\beta\alpha(ijk)}$ of the form

$$Q_{\beta\alpha(ijk)} = \int_{\Gamma_j} p^{\mathbf{n}*}_{\beta\alpha}(x,z,x_{\xi_i},z_{\xi_i},-k_y,\omega) S_{jk}(x,z)\, d\Gamma \tag{39}$$

and $\mathbf{H}$ is a matrix that collects the coefficients $H_{\beta\alpha(ijk)}$ of the form

$$H_{\beta\alpha(ijk)} = \int_{\Gamma_j} u_{\beta\alpha}(x,z,x_{\xi_i},z_{\xi_i},-k_y,\omega) S_{jk}(x,z)\, d\Gamma \tag{40}$$

In Eqs. (39) and (40), i represents the index of the collocation point $\mathbf{x}_{\xi_i}$, j represents the index of the boundary division Γ_j and $S_{jk}(\ldots)$ represents the shape function associated with the kth node of Γ_j.

In the following two sections, it is demonstrated that the coefficients $H_{\beta\alpha(ijk)}$ and $Q_{\beta\alpha(ijk)}$ for horizontal and for vertical boundary elements can be calculated directly with the TLM without the need for any kind of spatial integration scheme. For each orientation of the boundary element, it is also explained how to account for the term $c_{\alpha\beta}$.

3.1. Horizontal boundaries

Horizontal boundaries are defined by a constant depth. If it is assumed that the load is applied at depth z_n (nth interface of the TLM model) and that the boundary element is at depth z_m (mth interface of the TLM model), then the integrals in Eqs. (39) and (40) can be replaced by integrals of the form (for convenience, the indexes i, j, k and the variables k_y, ω are dropped)

$$H_{\alpha\beta} = \int_{\Gamma_j} u^{(mn)}_{\alpha\beta}(x - x_\xi) S(x)\, dx \tag{41}$$

$$Q_{\alpha\beta} = \int_{\Gamma_j} p^{(mn)}_{\alpha\beta}(x - x_\xi) S(x)\, dx \tag{42}$$

The variables $u^{(mn)}_{\alpha\beta}$ in Eq. (41) are defined in Section 2 and the variables $p^{(mn)}_{\alpha\beta}$ in Eq. (42) correspond to the components of the internal stresses in a horizontal plane, i.e., $p^{(mn)}_{\alpha\beta} = \pm\sigma^{(mn)}_{\alpha z\beta}$ (the positive sign is used when the outwards normal of the boundary faces the positive z direction, while the negative sign is used otherwise).

In order to complete the analytical evaluation of the integrals, Eq. (41) is first changed into a more convenient form. As seen in Section 2.4, the fundamental displacements are obtained through the inversion of the solutions in the wavenumber domain, i.e.,

$$u^{(mn)}_{\alpha\beta}(x) = \frac{1}{2\pi} \int_{-\infty}^{+\infty} \overline{u}^{(mn)}_{\alpha\beta}(k_x) e^{-ik_x x}\, dk_x \tag{43}$$

Assuming that the x axis is centered at the midpoint of the boundary element (of total width l), after substituting Eq. (43) into Eq. (41), the latter becomes

$$\begin{aligned} H_{\alpha\beta} &= \int_{-l/2}^{l/2} \frac{1}{2\pi} \int_{-\infty}^{+\infty} \overline{u}^{(mn)}_{\alpha\beta}(k_x) e^{-ik_x(x - x_\xi)}\, dk_x S(x)\, dx \\ &= \frac{1}{2\pi} \int_{-\infty}^{+\infty} \overline{u}^{(mn)}_{\alpha\beta}(k_x) \int_{-l/2}^{l/2} S(x) e^{-ik_x x}\, dx\, e^{ik_x x_\xi}\, dk_x \end{aligned} \tag{44}$$

The Fourier transform of $S(x)$ is defined by

$$\tilde{S}(k_x) = \int_{-\infty}^{+\infty} S(x) e^{-ik_x x}\, dx = \int_{-l/2}^{l/2} S(x) e^{-ik_x x}\, dx \tag{45}$$

and after introducing this in Eq. (44) we obtain

$$H_{\alpha\beta} = \frac{1}{2\pi} \int_{-\infty}^{+\infty} \overline{u}^{(mn)}_{\alpha\beta}(k_x) \tilde{S}(k_x)\, e^{ik_x x_\xi}\, dk_x \tag{46}$$

The application of the same procedure to Eq. (42) yields

$$Q_{\alpha\beta} = \frac{1}{2\pi}\int_{-\infty}^{+\infty} \pm\overline{\sigma}_{\alpha z\beta}^{(mn)}(k_x)\tilde{S}(k_x)\, e^{ik_x x_\xi} dk_x \tag{47}$$

The variable $\overline{u}_{\alpha\beta}^{(mn)}(k_x)$ is calculated by modal superposition. If the horizontal boundary is placed at the interface between two thin-layers (a condition that is assumed to be true throughout the remainder of the formulation), then $\overline{\sigma}_{\alpha z\beta}^{(mn)}$ corresponds to the consistent nodal tractions at that interface and thus $\overline{\sigma}_{\alpha z\beta}^{(mn)}(k_x)$ can also be obtained by modal superposition – Eqs. (8)–(16). For these reasons, if $\tilde{S}(k_x)$ can be expressed analytically (e.g., when $S(x)$ is a polynomial function), then $H_{\alpha\beta}$ and $Q_{\alpha\beta}$ can also be obtained analytically by modal superposition. This idea is explored next for $S(x) = S_j(x) = x^j,\ j = 0, 1, 2,$ but first observe that even though $u_{\alpha\beta}^{(mn)}(x)$ and $\sigma_{\alpha z\beta}^{(mn)}(x)$ become singular when $x \to 0$, the variables $\overline{u}_{\alpha\beta}^{(mn)}(k_x)$ and $\overline{\sigma}_{\alpha z\beta}^{(mn)}(k_x)$ are finite, and therefore the values of $H_{\alpha\beta}$ and $Q_{\alpha\beta}$ calculated with Eqs. (46) and (47) are also finite. Hence, when the collocation point belongs to the horizontal boundary element, $Q_{\alpha\beta}$ already includes the factor $c_{\alpha\beta}$. In other words, using the proposed procedure, Eq. (35) can be used directly in place of the regularized Eq. (37), with the term $c_{\alpha\beta}$ being automatically accounted for.

3.1.1. Constant shape function $S_0(x) = 1$

The Fourier transform of $S_0(x)$, according to Eq. (45), is

$$\tilde{S}_0(k_x) = \int_{-l/2}^{l/2} e^{-ik_x x} dx = -\frac{i}{k_x}\left(e^{i\frac{k_x l}{2}} - e^{-i\frac{k_x l}{2}}\right) \tag{48}$$

The coefficients $H_{\alpha\beta}$ are then obtained with

$$H_{\alpha\beta} = \frac{1}{2\pi}\int_{-\infty}^{+\infty} -\frac{i}{k_x}\overline{u}_{\alpha\beta}^{(mn)}\left[e^{ik_x\left(x_\xi+\frac{l}{2}\right)} - e^{ik_x\left(x_\xi-\frac{l}{2}\right)}\right] dk_x \tag{49}$$

and the coefficients $Q_{\alpha\beta}$ with

$$Q_{\alpha\beta} = \frac{1}{2\pi}\int_{-\infty}^{+\infty} -\frac{i}{k_x}\overline{\sigma}_{\alpha z\beta}^{(mn)}\left[e^{ik_x\left(x_\xi+\frac{l}{2}\right)} - e^{ik_x\left(x_\xi-\frac{l}{2}\right)}\right] dk_x \tag{50}$$

Defining the integrals

$$H_{\alpha\beta}^{(p)}(x) = \frac{1}{2\pi}\int_{-\infty}^{+\infty} k_x^p \overline{u}_{\alpha\beta}^{(mn)}\, e^{-ik_x x} dk_x \tag{51}$$

$$Q_{\alpha\beta}^{(p)}(x) = \frac{1}{2\pi}\int_{-\infty}^{+\infty} k_x^p \overline{\sigma}_{\alpha z\beta}^{(mn)}\, e^{-ik_x x} dk_x \tag{52}$$

and replacing them in Eqs. (49) and (50), these become

$$H_{\alpha\beta} = -i\, H_{\alpha\beta}^{(-1)}\left(-x_\xi - \frac{l}{2}\right) + i\, H_{\alpha\beta}^{(-1)}\left(-x_\xi + \frac{l}{2}\right) \tag{53}$$

$$Q_{\alpha\beta} = -i\, Q_{\alpha\beta}^{(-1)}\left(-x_\xi - \frac{l}{2}\right) + i\, Q_{\alpha\beta}^{(-1)}\left(-x_\xi + \frac{l}{2}\right) \tag{54}$$

In order to obtain $H_{\alpha\beta}^{(-1)}(x)$, the integrals $I_{ij}^{(-1)}$ defined by

$$I_{ij}^{(-1)} = \frac{1}{2\pi}\int_{-\infty}^{+\infty} k_x^{-1} K_{ij} e^{-ik_x x} dk_x \tag{55}$$

must be combined in a modal summation similar to the one described in Section 2. For example, $H_{xx}^{(-1)}(x)$ is calculated with

$$\begin{aligned} H_{xx}^{(-1)}(x) &= \frac{1}{2\pi}\int_{-\infty}^{+\infty} \frac{\overline{u}_{xx}^{(mn)}}{k_x} e^{-ik_x x} dk_x \\ &= \sum_j^{N_R} I_{3j}^{(-1)}(x)\phi_{xj}^{(m)}\phi_{xj}^{(n)} + \sum_j^{N_L} I_{4j}^{(-1)}(x)\ \phi_{yj}^{(m)}\phi_{yj}^{(n)} \end{aligned} \tag{56}$$

For the calculation of $Q_{\alpha\beta}^{(-1)}(x)$, the integrals $I_{ij}^{(-1)},\ I_{ij}^{(0)}$ and $I_{ij}^{(1)}$ must be used in Eqs. (8)–(16) in place of $K_{ij},\ k_x K_{ij}$ and $k_x^2 K_{ij}$, respectively. For example, assuming that the interested consistent nodal tractions are those of the upper interface of a thin-layer and that $\beta = z$, then

$$\begin{bmatrix} \mathbf{p}_{(1)} = \begin{Bmatrix} Q_{xz}^{(-1)} \\ Q_{yz}^{(-1)} \\ Q_{zz}^{(-1)} \end{Bmatrix} \\ \vdots \\ \mathbf{p}_{(nn)} \end{bmatrix} = \begin{aligned} &\mathbf{A}_{xx}\left(\sum_{j=1}^{N_R}\phi_{zj}^{(n)}\begin{bmatrix}\Lambda_{jR}^{(z1)} & & \\ & \ddots & \\ & & \Lambda_{jR}^{(z1)}\end{bmatrix}\begin{bmatrix}\boldsymbol{\Phi}_{Rj}^{(l)} \\ \vdots \\ \boldsymbol{\Phi}_{Rj}^{(m)}\end{bmatrix}\right) \\ &+(k_y\mathbf{A}_{xy} + \mathbf{B}_x)\left(\sum_{j=1}^{N_R}\phi_{zj}^{(n)}\begin{bmatrix}\Lambda_{jR}^{(z0)} & & \\ & \ddots & \\ & & \Lambda_{jR}^{(z0)}\end{bmatrix}\begin{bmatrix}\boldsymbol{\Phi}_{Rj}^{(l)} \\ \vdots \\ \boldsymbol{\Phi}_{Rj}^{(m)}\end{bmatrix}\right) \\ &+\left(k_y^2\mathbf{A}_{yy} + k_y\mathbf{B}_y + \mathbf{G} - \omega^2\mathbf{M}\right)\left(\sum_{j=1}^{N_R}\phi_{zj}^{(n)}\begin{bmatrix}\Lambda_{jR}^{(z,-1)} & & \\ & \ddots & \\ & & \Lambda_{jR}^{(z,-1)}\end{bmatrix}\begin{bmatrix}\boldsymbol{\Phi}_{Rj}^{(l)} \\ \vdots \\ \boldsymbol{\Phi}_{Rj}^{(m)}\end{bmatrix}\right) \end{aligned} \tag{57}$$

with $\Lambda_{jR}^{(zp)}$ as defined in Eq. (34). The integrals $I_{ij}^{(-1)},\ I_{ij}^{(0)}$ and $I_{ij}^{(1)}$ are listed in Appendix B.

3.1.2. Linear shape function $S_1(x) = x$

Following the procedure described in Section 3.1.1, the Fourier transform of $S_1(x)$ is

$$\begin{aligned} \tilde{S}_1(k_x) &= \int_{-l/2}^{l/2} x\, e^{-ik_x x} dx \\ &= \frac{l}{2}\frac{i}{k_x}\left(e^{i\frac{k_x l}{2}} + e^{-i\frac{k_x l}{2}}\right) + \frac{1}{k_x^2}\left(e^{-i\frac{k_x l}{2}} - e^{i\frac{k_x l}{2}}\right) \end{aligned} \tag{58}$$

and thus the coefficients $H_{\alpha\beta}$ and $Q_{\alpha\beta}$ are calculated with

$$\begin{aligned} H_{\alpha\beta} = \frac{il}{2}&\left\{H_{\alpha\beta}^{(-1)}\left(-x_\xi - \frac{l}{2}\right) + H_{\alpha\beta}^{(-1)}\left(-x_\xi + \frac{l}{2}\right)\right\} \\ &+ H_{\alpha\beta}^{(-2)}\left(-x_\xi + \frac{l}{2}\right) - H_{\alpha\beta}^{(-2)}\left(-x_\xi - \frac{l}{2}\right) \end{aligned} \tag{59}$$

$$\begin{aligned} Q_{\alpha\beta} = \frac{il}{2}&\left\{Q_{\alpha\beta}^{(-1)}\left(-x_\xi - \frac{l}{2}\right) + Q_{\alpha\beta}^{(-1)}\left(-x_\xi + \frac{l}{2}\right)\right\} \\ &+ Q_{\alpha\beta}^{(-2)}\left(-x_\xi + \frac{l}{2}\right) - Q_{\alpha\beta}^{(-2)}\left(-x_\xi - \frac{l}{2}\right) \end{aligned} \tag{60}$$

Expressions for the evaluation of $H_{\alpha\beta}^{(-1)}(x)$ and $Q_{\alpha\beta}^{(-1)}(x)$ are given in Section 3.1.1. In order to evaluate $H_{\alpha\beta}^{(-2)}(x)$ and $Q_{\alpha\beta}^{(-2)}(x)$, the integrals $I_{ij}^{(-2)},\ I_{ij}^{(-1)}$ and $I_{ij}^{(0)}$ must be used in the modal summations explained in Sections 2.1 and 2.2 in place of $K_{ij},\ k_x K_{ij}$ and $k_x^2 K_{ij}$, respectively. The expression for $I_{ij}^{(-2)}$ is

$$I_{ij}^{(-2)} = \frac{1}{2\pi}\int_{-\infty}^{+\infty} k_x^{-2} K_{ij} e^{-ik_x x} dk_x \tag{61}$$

The integrals $I_{ij}^{(-2)},\ I_{ij}^{(-1)}$ and $I_{ij}^{(0)}$ are listed in Appendix B.

3.1.3. Quadratic shape function $S_2(x) = x^2$

The Fourier transform of S_2 is

$$\begin{aligned} \tilde{S}_2(k_x) &= \int_{-l/2}^{l/2} x^2\, e^{-ik_x x} dx = -\frac{l^2 i}{4k_x}\left(e^{i\frac{k_x l}{2}} - e^{-i\frac{k_x l}{2}}\right) \\ &\quad + \frac{l}{k_x^2}\left(e^{i\frac{k_x l}{2}} + e^{-i\frac{k_x l}{2}}\right) + \frac{2i}{k_x^3}\left(e^{i\frac{k_x l}{2}} - e^{-i\frac{k_x l}{2}}\right) \end{aligned} \tag{62}$$

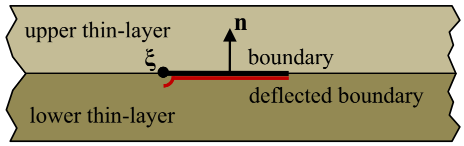

Fig. 3. Deflection of the horizontal boundary (red line) when the collocation point is at an edge of the element. (For interpretation of the references to color in this figure legend, the reader is referred to the web version of this article.)

and so the coefficients $H_{\alpha\beta}$ and $Q_{\alpha\beta}$ are obtained with

$$\begin{aligned}H_{\alpha\beta} = &-\frac{il^2}{4}\left\{H_{\alpha\beta}^{(-1)}\left(-x_\xi-\frac{l}{2}\right)-H_{\alpha\beta}^{(-1)}\left(-x_\xi+\frac{l}{2}\right)\right\}\\&+l\left\{H_{\alpha\beta}^{(-2)}\left(-x_\xi-\frac{l}{2}\right)+H_{\alpha\beta}^{(-2)}\left(-x_\xi+\frac{l}{2}\right)\right\}\\&+2i\left\{H_{\alpha\beta}^{(-3)}\left(-x_\xi-\frac{l}{2}\right)-H_{\alpha\beta}^{(-3)}\left(-x_\xi+\frac{l}{2}\right)\right\}\end{aligned} \tag{63}$$

$$\begin{aligned}Q_{\alpha\beta} = &-\frac{il^2}{4}\left\{Q_{\alpha\beta}^{(-1)}\left(-x_\xi-\frac{l}{2}\right)-Q_{\alpha\beta}^{(-1)}\left(-x_\xi+\frac{l}{2}\right)\right\}\\&+l\left\{Q_{\alpha\beta}^{(-2)}\left(-x_\xi-\frac{l}{2}\right)+Q_{\alpha\beta}^{(-2)}\left(-x_\xi+\frac{l}{2}\right)\right\}\\&+2i\left\{Q_{\alpha\beta}^{(-3)}\left(-x_\xi-\frac{l}{2}\right)-Q_{\alpha\beta}^{(-3)}\left(-x_\xi+\frac{l}{2}\right)\right\}\end{aligned} \tag{64}$$

Expressions for $H_{\alpha\beta}^{(-1)}(x)$, $H_{\alpha\beta}^{(-2)}(x)$, $Q_{\alpha\beta}^{(-1)}(x)$ and $Q_{\alpha\beta}^{(-2)}(x)$ are already given in Sections 3.1.1 and 3.1.2. To evaluate $H_{\alpha\beta}^{(-3)}(x)$ and $Q_{\alpha\beta}^{(-3)}(x)$, the integrals $I_{ij}^{(-3)}$, $I_{ij}^{(-2)}$ and $I_{ij}^{(-1)}$ must be used in the modal summations explained in Sections 2.1 and 2.2 in place of K_{ij}, k_xK_{ij} and $k_x^2K_{ij}$, respectively. The expression for $I_{ij}^{(-3)}$ is

$$I_{ij}^{(-3)} = \frac{1}{2\pi}\int_{-\infty}^{+\infty} k_x^{-3}K_{ij}e^{-ik_xx}dk_x \tag{65}$$

The integrals $I_{ij}^{(-3)}$, $I_{ij}^{(-2)}$ and $I_{ij}^{(-1)}$ are listed in Appendix B.

3.1.4. Final considerations concerning horizontal boundaries

The calculation of the coefficients $H_{\alpha\beta}$ involves only the components of the modal shapes at the elevation of the load and at the elevation of the receiver. By contrast, the calculation of the coefficients $Q_{\alpha\beta}$ involves the components of all TLM nodes that compose the thin-layer delimiting the boundary element. Since the boundary elements are placed at the interface between two consecutive thin-layers, a decision is required as to whether to consider the upper or the lower thin-layer.

When the collocation point is not contained by the boundary element, it is immaterial which thin-layer is used. On the other hand, when the collocation point is contained in the boundary element, the value of $Q_{\alpha\beta}$ depends on the thin-layer selected for the evaluation. The rule used in this work is that if the outward normal faces up, the thin-layer located below the boundary is employed in the calculation of $Q_{\alpha\beta}$, otherwise the thin-layer above is used. By following this procedure, collocation points on horizontal boundaries are circumvented as depicted in Fig. 2.

It is important to note that, according to this procedure, when a collocation point is at an edge of a boundary element ($x_\xi = \pm l/2$), then the coefficient $Q_{\alpha\beta}$ is calculated considering that the boundary is distorted as shown in Fig. 3. This aspect is important for the treatment of corners, i.e., points where horizontal boundaries meet vertical boundaries (Fig. 2b and c).

3.2. Vertical boundaries

Vertical boundaries are defined by a constant horizontal coordinate x_{BE}. If it is assumed that the load is applied at the depth z_l (lth interface of the TLM model) and that the boundary element is placed between depths z_m and z_n (mth and nth interfaces of the TLM model), then the integrals in Eqs. (39) and (40) can be replaced by integrals of the form (for convenience, the indexes i, j, k and the variables k_y, ω are dropped)

$$H_{\alpha\beta} = \sum_{p=m}^{n}\int u_{\alpha\beta}^{(pl)}(x_{BE}-x_\xi)N_p(z)S(z)dz \tag{66}$$

$$Q_{\alpha\beta} = \sum_{p=m}^{n}\int p_{\alpha\beta}^{(pl)}(x_{BE}-x_\xi)N_p(z)S(z)dz \tag{67}$$

In these equations, the factors $u_{\alpha\beta}^{(pl)}(x_{BE}-x_\xi)N_p(z)$ and $p_{\alpha\beta}^{(pl)}(x_{BE}-x_\xi)N_p(z)$ represent the vertically interpolated displacement and traction fields, with $N_p(z)$ being the shape function associated with the pth interface.

Since $u_{\alpha\beta}^{(pl)}(x_{BE}-x_\xi)$ and $p_{\alpha\beta}^{(pl)}(x_{BE}-x_\xi)$ are nodal values and therefore do not depend on the depth z, Eqs. (66) and (67) can be replaced by

$$H_{\alpha\beta} = \sum_{p=m}^{n}u_{\alpha\beta}^{(pl)}(x_{BE}-x_\xi)\int N_p(z)S(z)dz \tag{68}$$

$$Q_{\alpha\beta} = \sum_{p=m}^{n}p_{\alpha\beta}^{(pl)}(x_{BE}-x_\xi)\int N_p(z)S(z)dz \tag{69}$$

Thus, only the integrals of the form $\int N_p(z)S(z)dz$ need to be evaluated. Since $N_p(z)$ and $S(z)$ are both polynomial functions, these integrals can be evaluated in closed form.

In Eq. (68), $u_{\alpha\beta}^{(pl)}$ represents the nodal values of the displacements, which are calculated as explained in Section 2.4, and in Eq. (69), the tractions $p_{\alpha\beta}^{(pl)}$ correspond to the internal stresses in a vertical plane, i.e.,

$$p_{\alpha\beta}^{(pl)} = \pm\sigma_{\alpha x\beta}^{(pl)} \tag{70}$$

(the positive sign must be used if the outwards normal faces the positive x direction and the negative sign otherwise). The components of the internal stresses are calculated with

$$\begin{cases}\sigma_{xx\beta}^{(pl)} = \lambda\left(u_{x\beta,x}^{(pl)}+u_{y\beta,y}^{(pl)}+u_{z\beta,z}^{(pl)}\right)+2Gu_{x\beta,x}^{(pl)}\\ \sigma_{yx\beta}^{(pl)} = G\left(u_{x\beta,y}^{(pl)}+u_{y\beta,x}^{(pl)}\right)\\ \sigma_{zx\beta}^{(pl)} = G\left(u_{x\beta,z}^{(pl)}+u_{z\beta,x}^{(pl)}\right)\end{cases} \tag{71}$$

where the derivatives (both horizontal and vertical) are calculated as already explained in Sections 2.3 and 2.4.

As a final note, since the displacements are interpolated in the vertical direction using polynomial functions, the singular behavior of the GF is not captured. Hence, when the collocation point lies within the vertical boundary element, in the calculation of $Q_{\alpha\beta}$ the term $c_{\alpha\beta}$ is not accounted for. Nonetheless, since the boundary elements are vertically oriented and the GF are symmetric with respect to vertical planes, the resulting value for the missing term is $c_{\alpha\beta} = 0.5\delta_{\alpha\beta}$. In this way, for nodes that belong to vertical boundary elements and that do not correspond to corners, the term $c_{\alpha\beta} = 0.5\delta_{\alpha\beta}$ must be added to the diagonal of $\mathbf{Q}$ associated with the node. When the node corresponds to a corner, two situations occur:

1. Concave corner (Fig. 2b) – in this case, because the horizontal boundary element already accounts for the quarter circle of the deflected boundary (Fig. 3), then the factor $c_{\alpha\beta}$ must only account for the remaining semi-circle, and so $c_{\alpha\beta} = 0.5\delta_{\alpha\beta}$;
2. Convex corner (Fig. 2c) – the horizontal boundary element already accounts for the quarter circle of the deflected boundary (Fig. 3), and so the factor $c_{\alpha\beta}$ is null.

4. Validation examples

In the present section, the dynamic compliances of a tunnel are computed and compared with the corresponding values obtained with the 2.5D finite element method (FEM). The tunnel is massless, has rigid cross section, and is placed inside a horizontally layered domain. The geometry and properties of the problem are illustrated in Fig. 4.

Since the cross section of the tunnel is rigid, the displacements of the walls of the tunnel can be described as functions of the translations and rotations of the tunnel, i.e.,

$$\begin{bmatrix} u_x(x,z) \\ u_y(x,z) \\ u_z(x,z) \end{bmatrix} = \mathbf{N}\mathbf{U}^{\text{Tunnel}} \quad \mathbf{N} = \begin{bmatrix} 1 & 0 & 0 & 0 & z & 0 \\ 0 & 1 & 0 & -z & 0 & x \\ 0 & 0 & 1 & 0 & -x & 0 \end{bmatrix} \quad \mathbf{U}^{\text{Tunnel}} = \begin{bmatrix} u_x^{\text{Tunnel}} \\ u_y^{\text{Tunnel}} \\ u_z^{\text{Tunnel}} \\ \theta_x^{\text{Tunnel}} \\ \theta_y^{\text{Tunnel}} \\ \theta_z^{\text{Tunnel}} \end{bmatrix} \tag{72}$$

On the other hand, the pressures that the layered domain transmits to the walls of the tunnel induce at the center of the tunnel forces and moments that are calculated with

$$\mathbf{F}^{\text{Tunnel}} = [F_x \quad F_y \quad F_z \quad M_x \quad M_y \quad M_z]^{\text{T}} = \int_\Gamma \mathbf{N}^{\text{T}} \begin{bmatrix} p_x(x,z) \\ p_y(x,z) \\ p_z(x,z) \end{bmatrix} d\Gamma \tag{73}$$

where Γ represents the boundary of the tunnel.

After discretizing into boundary elements and N boundary nodes the surface of the layered domain that is in contact with the tunnel, the nodal displacements $\mathbf{u}_j$ at the boundary are obtained with

$$\begin{bmatrix} \mathbf{u}_1 \\ \vdots \\ \mathbf{u}_N \end{bmatrix} = \mathbf{N}_{\text{U}}\mathbf{U}^{\text{Tunnel}} \qquad \mathbf{N}_{\text{U}} = \begin{bmatrix} \mathbf{N}(x_1, z_1) \\ \vdots \\ \mathbf{N}(x_N, z_N) \end{bmatrix} \tag{74}$$

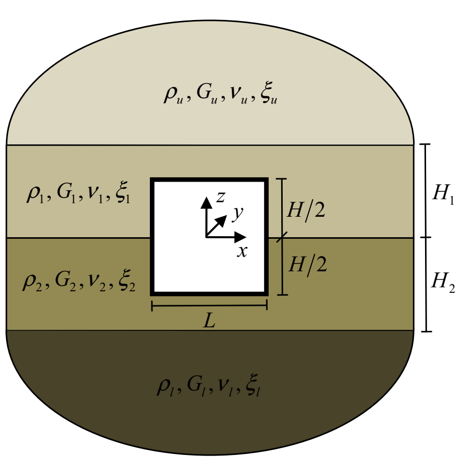

Fig. 4. Square tunnel inside a horizontally layered domain.

The forces $\mathbf{F}^{\text{Tunnel}}$ are obtained from the boundary pressures $\mathbf{p}_j$ through

$$\mathbf{F}^{\text{Tunnel}} = \mathbf{N}_{\text{P}} \begin{bmatrix} \mathbf{p}_1 \\ \vdots \\ \mathbf{p}_N \end{bmatrix} \mathbf{N}_{\text{P}} = \left[\int_\Gamma \mathbf{N}^{\text{T}}(x,z) S_1(x,z) d\Gamma \ \cdots \ \int_\Gamma \mathbf{N}^{\text{T}}(x,z) S_N(x,z) d\Gamma \right] \tag{75}$$

with $S_j(x,z)$ being the shape function associated with the jth boundary node.

Replacing Eqs. (74) and (75) in Eq. (38) yields

$$\left(\mathbf{N}_{\text{P}}\mathbf{H}^{-1}(\mathbf{C}+\mathbf{Q})\mathbf{N}_{\text{U}} \right) \mathbf{U}^{\text{Tunnel}} = \mathbf{F}^{\text{Tunnel}} \tag{76}$$

and so the compliance matrix is the 6 by 6 matrix $\mathbf{F}$ obtained with

$$\mathbf{F} = \left(\mathbf{N}_{\text{P}}\mathbf{H}^{-1}(\mathbf{C}+\mathbf{Q})\mathbf{N}_{\text{U}} \right)^{-1} \tag{77}$$

In the subsequent examples, the components of the compliance matrix $\mathbf{F}$ are evaluated using the methodology explained earlier in this work. The tunnel is given the cross section $H = L = 1$ [m] and each edge of the tunnel is divided into 5 boundary elements of quadratic expansion (3 nodes per boundary element). The total number of nodes is then $N = 40$. The excitation frequency is $\omega = 2\pi$ [rad/s] and the wavenumbers k_y range from 0 to 6π [rad/m] (301 wavenumbers).

To validate the results obtained with the 2.5D BEM, the compliance matrices are also calculated using the FEM (the 2.5D FEM procedure used in this work was implemented by the authors). The corresponding model consists of an elastic region surrounded by PMLs, whose objective is to absorb outgoing waves (Fig. 5a). The thickness of each PML is two times the characteristic wavelength (taken as the shear wavelength of the stiffest layer), and the corresponding absorption profile is defined as explained in Ref. [21]. The mesh used to describe the domain is regular, consisting of rectangular shaped elements with 9 nodes each (usually, 2D quadrilateral elements of quadratic interpolation contain 8 nodes; here, a node is added at the center of the element). The mesh refinement is such that in the elastic region there are 20 elements (40 nodes) per wavelength and that in PMLs there are 10 elements (20 nodes) per wavelength. The mesh structure is represented in Fig. 5b (depending on the example being solved, the upper and/or lower PMLs may be excluded from the analysis).

4.1. Homogeneous whole-space

The material properties of the whole-space are: mass density $\rho_u = \rho_1 = \rho_2 = \rho_l = 1$ [kg/m^3]; shear modulus $G_u = G_1 = G_2 = G_l = 1$ [Pa]; Poisson's ratio $\nu_u = \nu_1 = \nu_2 = \nu_l = 0.25$; hysteretic damping ratio $\xi_u = \xi_1 = \xi_2 = \xi_l = 1\%$. The TLM model consists of the 4 macro-layers identified in Fig. 4, where the upper and lower semi-infinite elements are modeled with PMLs (with parameters $\eta = 2$, $\Omega = 8$, $N = 10$, $m = 2$; see [11] for the definition of these variables), and the middle layers satisfy $H_1 = H_2 = 2$[m] and are divided into 40 thin-layers of quadratic expansion ($nn = 3$).

Due to symmetry conditions, only the components f_{xx}, f_{yy}, f_{zz}, $f_{\theta_x\theta_x}$, $f_{\theta_y\theta_y}$, $f_{\theta_z\theta_z}$, $f_{x\theta_z} = -f_{\theta_z x}$ and $f_{z\theta_x} = -f_{\theta_x z}$ are non-zero. Also, due to the geometry of the problem, $f_{xx} = f_{zz}$, $f_{\theta_x\theta_x} = f_{\theta_z\theta_z}$ and $f_{x\theta_z} = f_{z\theta_x}$. Hence, considering only the five compliance components f_{xx}, f_{yy}, $f_{\theta_x\theta_x}$, $f_{\theta_y\theta_y}$ and $f_{x\theta_z}$ it is possible to describe the entire system. In Fig. 6, the five components of the compliance matrix obtained with the proposed procedure (solid lines) are compared with the results obtained with the finite element method (black dots). Blue is used for the representation of the real part, while red is used for the imaginary part [color on the online version only].

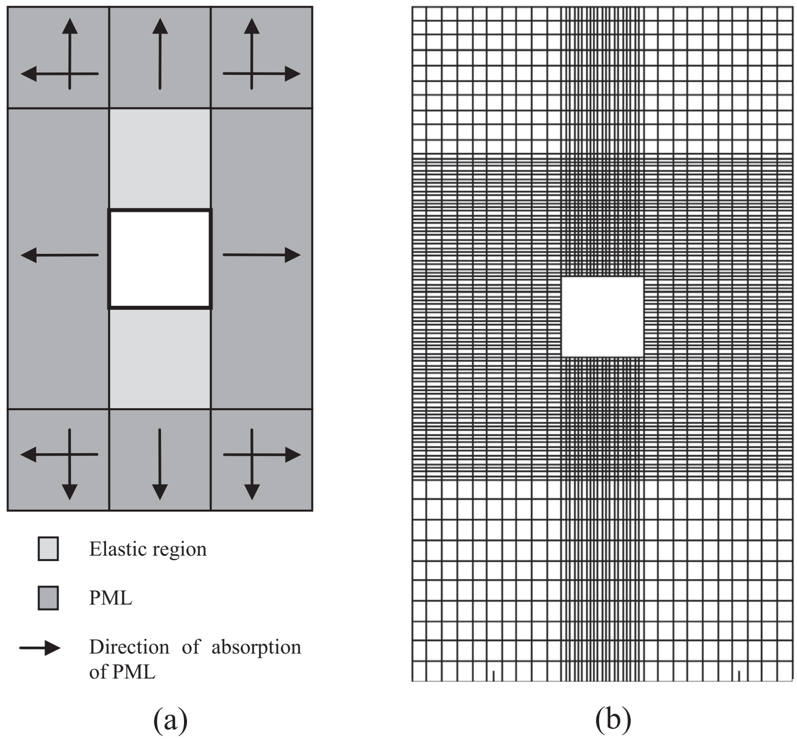

Fig. 5. (a) Scheme of the FEM + PML model. (b) FEM mesh.

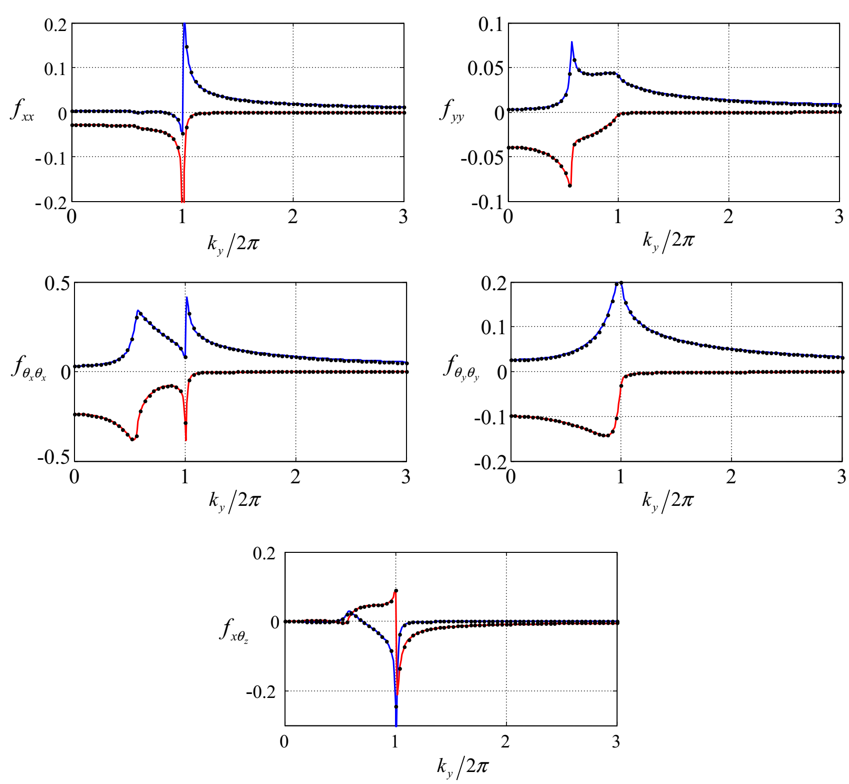

Fig. 6. Tunnel compliances for the case of a whole-space. Solid lines = 2.5D BEM (real part – blue; imaginary part – red). Black dots = FEM. (For interpretation of the references to color in this figure legend, the reader is referred to the web version of this article.)

Fig. 6 shows that the two approaches yield virtually identical results, leading to the conclusion that both procedures are correct. It can also be observed that the in-plane components (f_{xx}, $f_{\theta_x\theta_x}$ and $f_{x\theta_z}$) present singularities at $k_y = k_S = \omega/C_S = 2\pi$.

It should be noted that, because in this example the soil is a homogenous, infinite space, it follows that the classical BEM that uses the GF for that whole space has a clear advantage over the use of the BEM + TLM. However, this problem of very simple

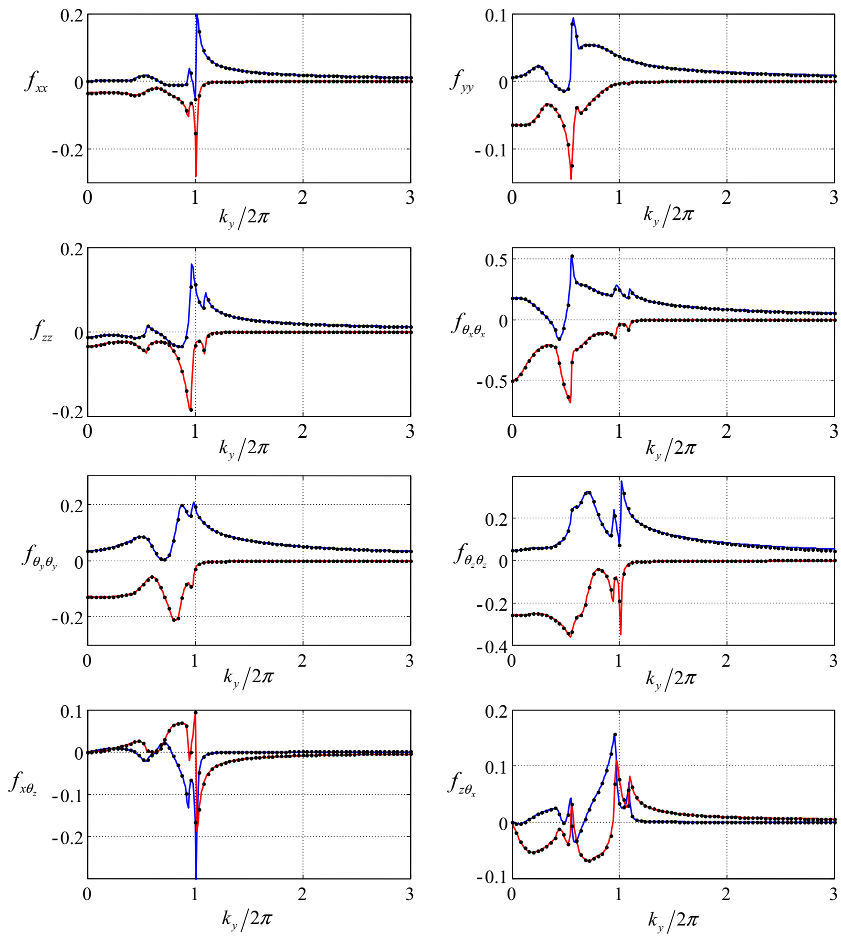

Fig. 7. Tunnel compliances for the case of a homogeneous layer free in space. Solid lines = 2.5D BEM (real part – blue; imaginary part – red). Black dots = FEM. (For interpretation of the references to color in this figure legend, the reader is referred to the web version of this article.)

geometry is used solely for validation purposes. In the next examples, the use of whole-space GF requires the discretization not only of the edges of the tunnel but also of the free-surfaces and of the interfaces between different layers, and now the TLM offers clear advantages inasmuch as these interfaces need not be discretized.

4.2. Homogeneous layer free in space

The free layer consists on the two intermediate macro layers depicted in Fig. 4 ($H_1 = H_2 = 2$ [m]). The material properties of the free layer are the same of the whole-space considered in the previous example. The TLM model is similar to the one used therein, but with the upper and lower PMLs excluded. Again, due to symmetry conditions, only the components f_{xx}, f_{yy}, f_{zz}, $f_{\theta_x\theta_x}$, $f_{\theta_y\theta_y}$, $f_{\theta_z\theta_z}$, $f_{x\theta_z} = -f_{\theta_z x}$ and $f_{z\theta_x} = -f_{\theta_x z}$ do not vanish. However, the identities $f_{xx} = f_{zz}$, $f_{\theta_x\theta_x} = f_{\theta_z\theta_z}$ and $f_{x\theta_z} = f_{z\theta_x}$ do not hold, and so a total of eight components of the compliance matrix are needed to describe the system. Fig. 7 shows the eight components of the compliance matrix obtained with the proposed methodology and with the FEM. Once again, the results obtained with the two procedures match perfectly.

4.3. Homogeneous half-space

The material properties of the homogeneous half-space are the same as in the previous case. The TLM model differs from the model in Section 4.1 in that the upper PML is excluded. In this case 12 distinct components are needed to define the compliance matrix, whose structure is

$$\mathbf{F} = \begin{bmatrix} f_{xx} & 0 & 0 & 0 & f_{x\theta_y} & f_{x\theta_z} \\ 0 & f_{yy} & f_{yz} & f_{y\theta_x} & 0 & 0 \\ 0 & -f_{yz} & f_{zz} & f_{z\theta_x} & 0 & 0 \\ 0 & f_{y\theta_x} & -f_{z\theta_x} & f_{\theta_x\theta_x} & 0 & 0 \\ f_{x\theta_y} & 0 & 0 & 0 & f_{\theta_y\theta_y} & f_{\theta_y\theta_z} \\ -f_{x\theta_z} & 0 & 0 & 0 & -f_{\theta_y\theta_z} & f_{\theta_z\theta_z} \end{bmatrix} \tag{78}$$

The diagonal components of $\mathbf{F}$ computed with the proposed procedure and with FEM are depicted in Fig. 8 and the off-diagonal components are shown in Fig. 9. A good agreement is reached, even though, for $k_y > 2\pi$, nearly imperceptible discrepancies can begin to be observed in Fig. 8 for the diagonal terms.

4.4. Layered half-space

The case of a non-homogeneous half-space is considered next. The properties of the layers, based on Fig. 4, are the following:

$$\rho_u = 0, G_u = 0 \quad \text{(the upper half-space does not exist in this case)}$$

$$\rho_1 = 1.2\ [\text{kg/m}^3], G_1 = 1.0\ [\text{Pa}], \nu_1 = 0.25, \xi_1 = 1\%, H_1 = 2\ [\text{m}]$$

$$\rho_2 = 1.3\ [\text{kg/m}^3], G_2 = 2.0\ [\text{Pa}], \nu_2 = 0.3, \xi_2 = 1\%, H_2 = 2\ [\text{m}]$$

$$\rho_l = \rho_2, G_l = G_2, \nu_l = \nu_2, \xi_l = \xi_2$$

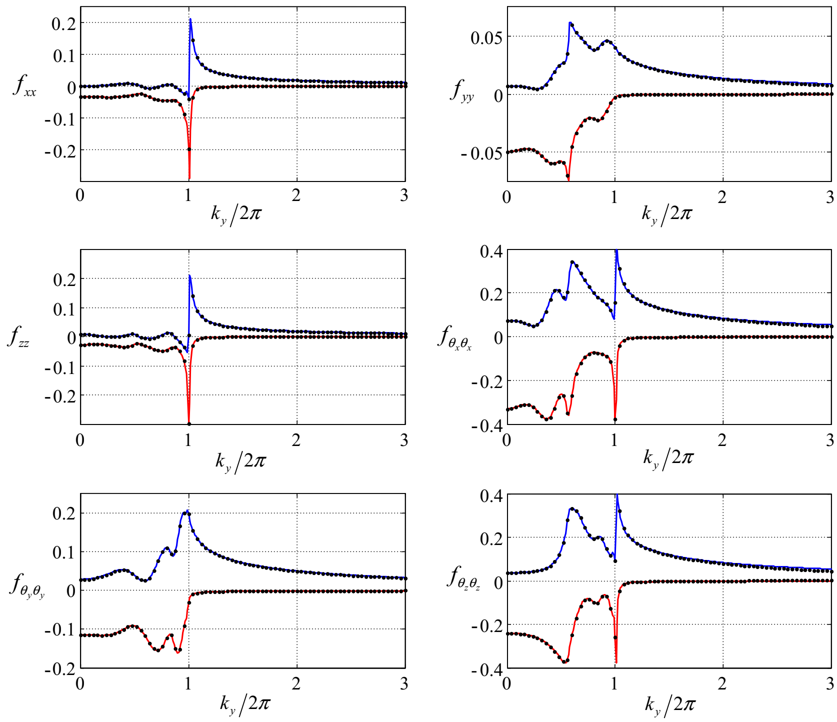

Fig. 8. Tunnel compliances (diagonal components) for the case of a homogeneous half-space. Solid lines = 2.5D BEM (real part – blue; imaginary part – red). Black dots = FEM. (For interpretation of the references to color in this figure legend, the reader is referred to the web version of this article.)

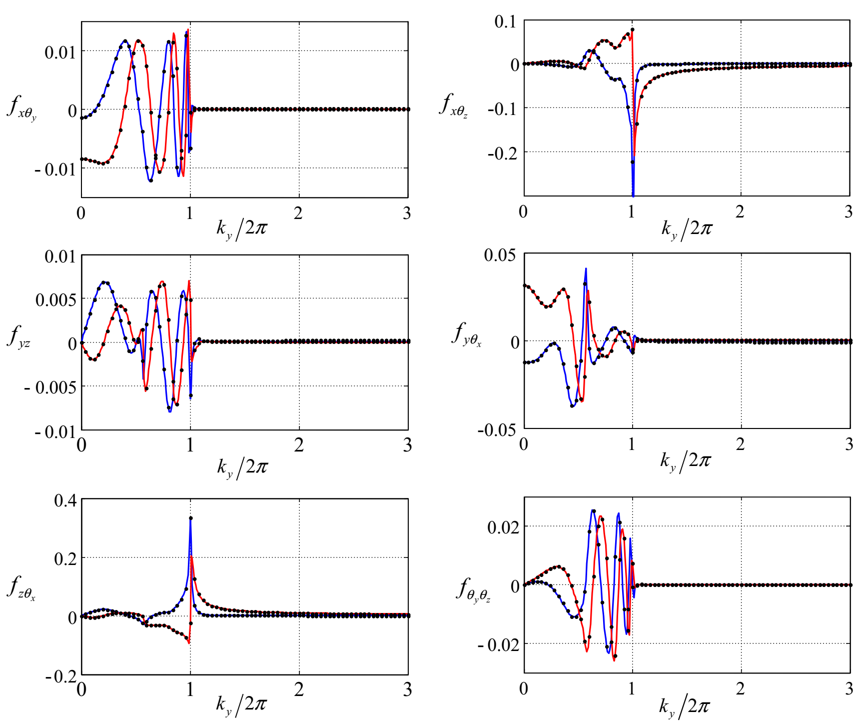

Fig. 9. Tunnel compliances (off-diagonal components) for the case of a homogeneous half-space. Solid lines = 2.5D BEM (real part – blue; imaginary part – red). Black dots = FEM. (For interpretation of the references to color in this figure legend, the reader is referred to the web version of this article.)

Each of the physical layers is modeled with 40 thin-layers based on a quadratic expansion ($nn = 3$). The lower half-space is modeled with PMLs with the same parameters used in Section 4.1 ($\eta = 2, \Omega = 8, N = 10, m = 2$).

As in the case of the half-space, the 12 components given by Eq. (78) are needed in order to define the compliance matrix **F**. These compliances, obtained both with the proposed procedure and with the FEM, are plotted in Fig. 10 for the diagonal components and in

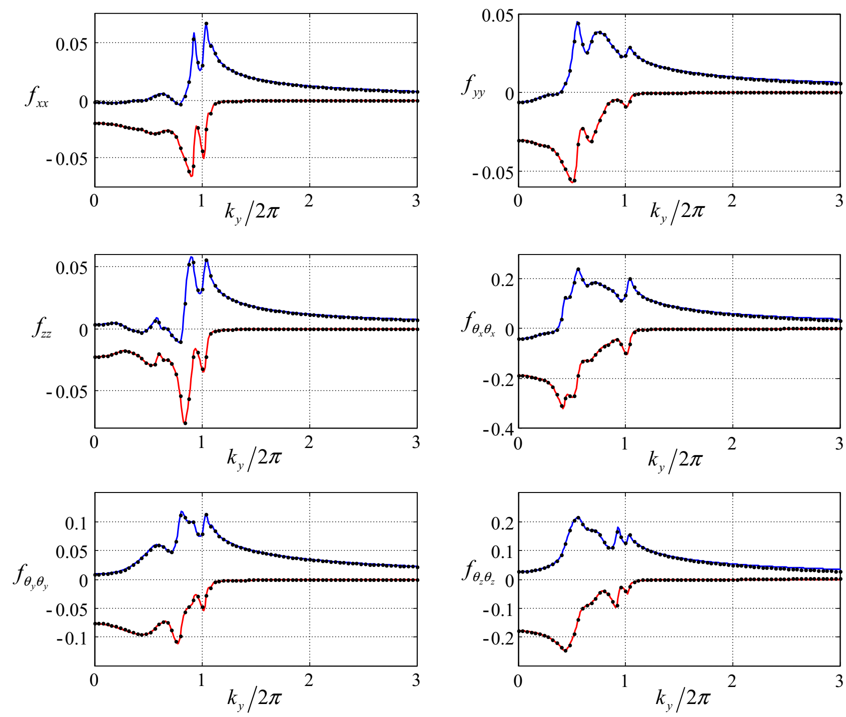

Fig. 10. Tunnel compliances (diagonal components) for the case of a layered half-space. Solid lines = 2.5D BEM (real part – blue; imaginary part – red). Black dots = FEM. (For interpretation of the references to color in this figure legend, the reader is referred to the web version of this article.)

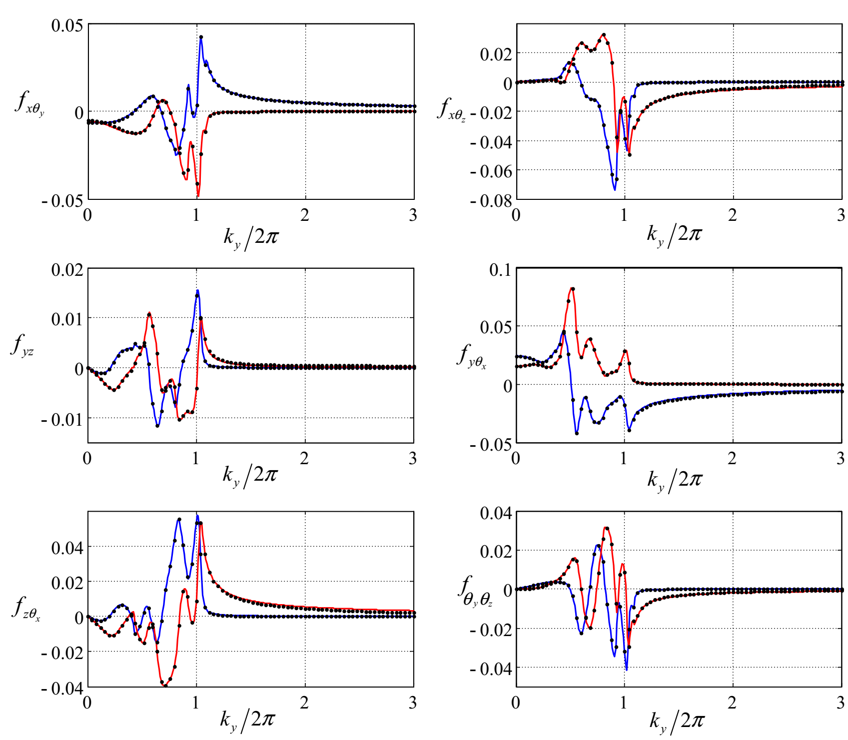

Fig. 11. Tunnel compliances (off-diagonal components) for the case of a layered half-space. Solid lines = 2.5D BEM (real part – blue; imaginary part – red). Black dots = FEM. (For interpretation of the references to color in this figure legend, the reader is referred to the web version of this article.)

Fig. 11 for the off-diagonal components. Again, the agreement between the proposed method and the FEM is very good. It can be concluded from this example that the BEM based on the TLM GF can correctly simulate horizontally layered domains without the need to discretize the interfaces between the layers, as is necessary in the standard BEM. This is a huge advantage.

5. Concluding remarks

In this article we presented a BEM procedure based on the TLM Green's functions. For horizontal boundary elements, the BEM coefficients are calculated directly based on a modal superposition, rendering accurate results and accounting for the singularities of the GF. For vertical boundary elements, the vertically interpolated GF are integrated analytically but the singularities are not accounted for: to account for the singular behavior of the GF, we need to add à *posteriori* the term $c_{\alpha\beta}$, which is equal to $0.5\delta_{\alpha\beta}$ in smooth vertical boundaries or concave corners and is null in convex corners.

The proposed methodology is limited to horizontal and vertical boundary elements. If the actual boundary should contain inclined surfaces, such geometry can be achieved by filling the irregular volume with finite elements. Other remarks concerning the compatibility between the TLM model and the BEM mesh are listed below:

1. The horizontal boundary elements are placed at the interface between two thin-layers and not inside a thin-layer.
2. The extremities of vertical boundary elements correspond to interfaces between thin-layers and not to intermediate elevations within thin-layers.
3. If there are boundary nodes inside vertical boundary elements (in constant or quadratic boundary elements, for example), these nodes must be located at the interface between thin-layers.
4. It is not recommended that the horizontal boundary elements be smaller than the thickness of the thin-layers. Likewise, it is not recommended that the distance between vertical boundary elements at the same level be smaller than the thickness of the thin-layers.

To the casual reader, the methodology presented in this article may seem complicated if not intimidating, but make no mistake, it is extremely powerful, inasmuch as it allows consideration of layered soils without the need to discretize the material interfaces (something which is not possible with the classical BEM based on the theoretical whole-space GF) and without the need to evaluate inverse Fourier transforms from k_x to x (which again is not possible in formulations based on GF obtained with stiffness/transfer matrices). In addition, the proposed methodology turns out to more user friendly than other procedures based on the stiffness/transfer matrices GFs since the definition of a proper wavenumber sample k_x is replaced by the subdivision of the layered domain into small thin-layers, a task that is far simple. For these reasons, it is believed that the methodology expounded herein constitutes an effective and fast alternative to assess the dynamic interaction of structures embedded in layered soils.

Acknowledgments

The first author wishes to thank the financial support he received from the *Fundação para a Ciência e a Tecnologia* of Portugal (FCT) through Grant No. SFRH/BD/47724/2008 and project number PTDC/ECM/114505/2009, and from the *Risk Assessment and Management for High-speed Rail Systems*' project of the MIT-Portugal Program in the Transportation Systems Area. This work was partially developed during the internship of the first author at MIT as a visiting student under the umbrella of the MIT-Portugal Program.

Appendix A. Thin layer matrices for cross anisotropy

The constitutive matrix $\mathbf{D}$ and the matrices $\mathbf{D}_{\alpha\beta}$ are defined by

$$\mathbf{D} = \begin{bmatrix} \lambda+2G & \lambda & \lambda_t & 0 & 0 & 0 \\ \lambda & \lambda+2G & \lambda_t & 0 & 0 & 0 \\ \lambda_t & \lambda_t & D_t & 0 & 0 & 0 \\ 0 & 0 & 0 & G_t & 0 & 0 \\ 0 & 0 & 0 & 0 & G_t & 0 \\ 0 & 0 & 0 & 0 & 0 & G \end{bmatrix} \quad \begin{array}{c} G>0 \\ G_t>0 \\ \lambda+G>0 \\ (\lambda+G)D_t>\lambda_t^2 \end{array}$$

$$\mathbf{D}_{xx} = \begin{bmatrix} \lambda+2G & 0 & 0 \\ 0 & G & 0 \\ 0 & 0 & G_t \end{bmatrix} \quad \mathbf{D}_{xy} = \begin{bmatrix} 0 & \lambda & 0 \\ G & 0 & 0 \\ 0 & 0 & 0 \end{bmatrix} \quad \mathbf{D}_{xz} = \begin{bmatrix} 0 & 0 & \lambda_t \\ 0 & 0 & 0 \\ G_t & 0 & 0 \end{bmatrix}$$

$$\mathbf{D}_{yx} = \begin{bmatrix} 0 & G & 0 \\ \lambda & 0 & 0 \\ 0 & 0 & 0 \end{bmatrix} \quad \mathbf{D}_{yy} = \begin{bmatrix} G & 0 & 0 \\ 0 & \lambda+2G & 0 \\ 0 & 0 & G_t \end{bmatrix} \quad \mathbf{D}_{yz} = \begin{bmatrix} 0 & 0 & 0 \\ 0 & 0 & \lambda_t \\ 0 & G_t & 0 \end{bmatrix}$$

$$\mathbf{D}_{zx} = \begin{bmatrix} 0 & 0 & G_t \\ 0 & 0 & 0 \\ \lambda_t & 0 & 0 \end{bmatrix} \quad \mathbf{D}_{zy} = \begin{bmatrix} 0 & 0 & 0 \\ 0 & 0 & G_t \\ 0 & \lambda_t & 0 \end{bmatrix} \quad \mathbf{D}_{zz} = \begin{bmatrix} G_t & 0 & 0 \\ 0 & G_t & 0 \\ 0 & 0 & D_t \end{bmatrix}$$

A.1. Linear expansion

The shape functions for this case are

$$N_1 = \zeta \qquad N_2 = 1-\zeta \qquad \zeta = z/h$$

where $z=0$ at the bottom surface of the thin-layer and $z=h$ at the top surface. The thin-layer matrices are

$$\mathbf{M} = \frac{\rho h}{6}\begin{bmatrix} 2\mathbf{I} & \mathbf{I} \\ \mathbf{I} & 2\mathbf{I} \end{bmatrix}$$

$$\mathbf{A}_{\alpha\alpha} = \frac{h}{6}\begin{bmatrix} 2\mathbf{D}_{\alpha\alpha} & \mathbf{D}_{\alpha\alpha} \\ \mathbf{D}_{\alpha\alpha} & 2\mathbf{D}_{\alpha\alpha} \end{bmatrix} \qquad (\alpha = x, y)$$

$$\mathbf{A}_{xy} = \frac{h}{6}\begin{bmatrix} 2(\mathbf{D}_{xy}+\mathbf{D}_{yx}) & (\mathbf{D}_{xy}+\mathbf{D}_{yx}) \\ (\mathbf{D}_{xy}+\mathbf{D}_{yx}) & 2(\mathbf{D}_{xy}+\mathbf{D}_{yx}) \end{bmatrix}$$

$$\mathbf{B}_{\alpha} = \frac{1}{2}\left(\begin{bmatrix} -\mathbf{D}_{\alpha z} & \mathbf{D}_{\alpha z} \\ -\mathbf{D}_{\alpha z} & \mathbf{D}_{\alpha z} \end{bmatrix} - \begin{bmatrix} -\mathbf{D}_{z\alpha} & -\mathbf{D}_{z\alpha} \\ \mathbf{D}_{z\alpha} & \mathbf{D}_{z\alpha} \end{bmatrix}\right) \qquad (\alpha = x, y)$$

$$\mathbf{G} = \frac{1}{h}\begin{bmatrix} \mathbf{D}_{zz} & -\mathbf{D}_{zz} \\ -\mathbf{D}_{zz} & \mathbf{D}_{zz} \end{bmatrix}$$

After assembling the elementary matrix $\mathbf{B}_{\alpha}$, the elementary matrix $\tilde{\mathbf{B}}_{\alpha}$ is obtained by changing the sign of every third column of $\mathbf{B}_{\alpha}$.

A.2. Quadratic expansion

The shape functions are now

$$N_1 = \zeta(2\zeta-1) \qquad N_2 = 4\zeta(1-\zeta) \qquad N_3 = (1-\zeta)(1-2\zeta)$$
$$\zeta = z/h$$

where again $z=0$ at the bottom surface of the thin-layer and $z=h$ at its top surface. The thin-layer matrices are

$$\mathbf{M}=\frac{\rho h}{30}\begin{bmatrix}4\mathbf{I} & 2\mathbf{I} & -\mathbf{I}\\ 2\mathbf{I} & 16\mathbf{I} & 2\mathbf{I}\\ -\mathbf{I} & 2\mathbf{I} & 4\mathbf{I}\end{bmatrix}$$

$$\mathbf{A}_{\alpha\alpha}=\frac{h}{30}\begin{bmatrix}4\mathbf{D}_{\alpha\alpha} & 2\mathbf{D}_{\alpha\alpha} & -\mathbf{D}_{\alpha\alpha}\\ 2\mathbf{D}_{\alpha\alpha} & 16\mathbf{D}_{\alpha\alpha} & 2\mathbf{D}_{\alpha\alpha}\\ -\mathbf{D}_{\alpha\alpha} & 2\mathbf{D}_{\alpha\alpha} & 4\mathbf{D}_{\alpha\alpha}\end{bmatrix}\qquad(\alpha=x,y)$$

$$\mathbf{A}_{xy}=\frac{h}{30}\begin{bmatrix}4(\mathbf{D}_{xy}+\mathbf{D}_{yx}) & 2(\mathbf{D}_{xy}+\mathbf{D}_{yx}) & -(\mathbf{D}_{xy}+\mathbf{D}_{yx})\\ 2(\mathbf{D}_{xy}+\mathbf{D}_{yx}) & 16(\mathbf{D}_{xy}+\mathbf{D}_{yx}) & 2(\mathbf{D}_{xy}+\mathbf{D}_{yx})\\ -(\mathbf{D}_{xy}+\mathbf{D}_{yx}) & 2(\mathbf{D}_{xy}+\mathbf{D}_{yx}) & 4(\mathbf{D}_{xy}+\mathbf{D}_{yx})\end{bmatrix}$$

$$\mathbf{B}_\alpha=\frac{1}{6}\left(\begin{bmatrix}3\mathbf{D}_{\alpha z} & -2\mathbf{D}_{\alpha z} & \mathbf{D}_{\alpha z}\\ 2\mathbf{D}_{\alpha z} & \mathbf{0} & -2\mathbf{D}_{\alpha z}\\ -\mathbf{D}_{\alpha z} & 2\mathbf{D}_{\alpha z} & -3\mathbf{D}_{\alpha z}\end{bmatrix}-\begin{bmatrix}3\mathbf{D}_{z\alpha} & 2\mathbf{D}_{z\alpha} & -\mathbf{D}_{z\alpha}\\ -2\mathbf{D}_{z\alpha} & \mathbf{0} & 2\mathbf{D}_{z\alpha}\\ \mathbf{D}_{z\alpha} & -2\mathbf{D}_{z\alpha} & -3\mathbf{D}_{z\alpha}\end{bmatrix}\right)\ (\alpha=x,y)$$

$$\mathbf{G}=\frac{1}{3h}\begin{bmatrix}7\mathbf{D}_{zz} & -8\mathbf{D}_{zz} & \mathbf{D}_{zz}\\ -8\mathbf{D}_{zz} & 16\mathbf{D}_{zz} & -8\mathbf{D}_{zz}\\ \mathbf{D}_{zz} & -8\mathbf{D}_{zz} & 7\mathbf{D}_{zz}\end{bmatrix}$$

Again, after assembling the elementary matrix $\mathbf{B}_\alpha$, the elementary matrix $\tilde{\mathbf{B}}_\alpha$ is obtained by changing the sign of every third column of $\mathbf{B}_\alpha$.

Appendix B. List of integrals

Closed form expressions for $I_{ij}^{(-3)}\ \left(Im\sqrt{k_j^2-k_y^2}<0\right)$

$$I_{1j}^{(-3)}=\frac{1}{2\pi}\int_{-\infty}^{+\infty}k_x^{-3}K_{1j}e^{-ik_xx}dk_x=-\frac{\operatorname{sign}(x)}{2i(k_y^2-k_j^2)}\left(\frac{x^2}{2}+\frac{1}{k_y^2-k_j^2}-\frac{e^{-i\sqrt{k_j^2-k_y^2}|x|}}{k_y^2-k_j^2}\right)$$

$$I_{2j}^{(-3)}=\frac{1}{2\pi}\int_{-\infty}^{+\infty}k_x^{-3}K_{2j}e^{-ik_xx}dk_x=\frac{1}{2k_y}\left\{\frac{-|x|}{k_y^2-k_j^2}+\frac{e^{-|k_yx|}}{|k_y|k_j^2}+i\frac{k_y^2e^{-i\sqrt{k_j^2-k_y^2}|x|}}{k_j^2(k_y^2-k_j^2)\sqrt{k_j^2-k_y^2}}\right\}$$

$$I_{3j}^{(-3)}=\frac{1}{2\pi}\int_{-\infty}^{+\infty}k_x^{-3}K_{3j}e^{-ik_xx}dk_x=\frac{\operatorname{sign}(x)}{2ik_y^2}\left\{\frac{1}{k_y^2-k_j^2}+\frac{e^{-|k_y\,x|}}{k_j^2}-\frac{k_y^2e^{-i\sqrt{k_j^2-k_y^2}\,|x|}}{k_j^2(k_y^2-k_j^2)}\right\}$$

$$I_{4j}^{(-3)}=\frac{1}{2\pi}\int_{-\infty}^{+\infty}k_x^{-3}K_{4j}e^{-ik_xx}dk_x=-\frac{\operatorname{sign}(x)}{2i}\left\{\frac{x^2}{2(k_y^2-k_j^2)}+\frac{2k_y^2-k_j^2}{k_y^2(k_y^2-k_j^2)^2}+\frac{e^{-|k_y\,x|}}{k_y^2k_j^2}-\frac{k_y^2e^{-i\sqrt{k_j^2-k_y^2}\,|x|}}{k_j^2(k_y^2-k_j^2)^2}\right\}$$

$$I_{5j}^{(-3)}=\frac{1}{2\pi}\int_{-\infty}^{+\infty}k_x^{-3}K_{5j}e^{-ik_xx}dk_x=-\frac{1}{2k_j(k_y^2-k_j^2)}\left(|x|-i\frac{e^{-i\sqrt{k_j^2-k_y^2}|x|}}{\sqrt{k_j^2-k_y^2}}\right)$$

$$I_{6j}^{(-3)}=\frac{1}{2\pi}\int_{-\infty}^{+\infty}k_x^{-3}K_{6j}e^{-ik_xx}dk_x=-\frac{\operatorname{sign}(x)k_y}{2ik_j(k_y^2-k_j^2)}\left(\frac{x^2}{2}+\frac{1}{k_y^2-k_j^2}-\frac{e^{-i\sqrt{k_j^2-k_y^2}|x|}}{k_y^2-k_j^2}\right)$$

Closed form expressions for $I_{ij}^{(-2)}\ \left(Im\sqrt{k_j^2-k_y^2}<0\right)$

$$I_{1j}^{(-2)}=\frac{1}{2\pi}\int_{-\infty}^{+\infty}k_x^{-2}K_{1j}e^{-ik_xx}dk_x=-\frac{1}{2(k_y^2-k_j^2)}\left(|x|-i\frac{e^{-i\sqrt{k_j^2-k_y^2}|x|}}{\sqrt{k_j^2-k_y^2}}\right)$$

$$I_{2j}^{(-2)}=\frac{1}{2\pi}\int_{-\infty}^{+\infty}k_x^{-2}K_{2j}e^{-ik_xx}dk_x=\frac{k_y\operatorname{sign}(x)}{2i}\left\{\frac{1}{k_y^2(k_y^2-k_j^2)}+\frac{e^{-|k_yx|}}{k_y^2k_j^2}-\frac{e^{-i\sqrt{k_j^2-k_y^2}|x|}}{k_j^2(k_y^2-k_j^2)}\right\}$$

$$I_{3j}^{(-2)}=\frac{1}{2\pi}\int_{-\infty}^{+\infty}k_x^{-2}K_{3j}e^{-ik_xx}dk_x=-\frac{1}{2k_j^2}\left(\frac{e^{-|k_yx|}}{|k_y|}+i\frac{e^{-i\sqrt{k_j^2-k_y^2}|x|}}{\sqrt{k_j^2-k_y^2}}\right)$$

$$I_{4j}^{(-2)}=\frac{1}{2\pi}\int_{-\infty}^{+\infty}k_x^{-2}K_{4j}e^{-ik_xx}dk_x=\frac{1}{2}\left\{\frac{-|x|}{k_y^2-k_j^2}+\frac{e^{-|k_yx|}}{|k_y|k_j^2}+i\frac{k_y^2e^{-i\sqrt{k_j^2-k_y^2}|x|}}{k_j^2(k_y^2-k_j^2)\sqrt{k_j^2-k_y^2}}\right\}$$

$$I_{5j}^{(-2)}=\frac{1}{2\pi}\int_{-\infty}^{+\infty}k_x^{-2}K_{5j}e^{-ik_xx}dk_x=\frac{\operatorname{sign}(x)}{2ik_j(k_y^2-k_j^2)}\left(1-e^{-i\sqrt{k_j^2-k_y^2}|x|}\right)$$

$$I_{6j}^{(-2)}=\frac{1}{2\pi}\int_{-\infty}^{+\infty}k_x^{-2}K_{6j}e^{-ik_xx}dk_x=-\frac{k_y}{2k_j(k_y^2-k_j^2)}\left(|x|-i\frac{e^{-i\sqrt{k_j^2-k_y^2}|x|}}{\sqrt{k_j^2-k_y^2}}\right)$$

Closed form expressions for $I_{ij}^{(-1)}\ \left(Im\sqrt{k_j^2-k_y^2}<0\right)$

$$I_{1j}^{(-1)}=\frac{1}{2\pi}\int_{-\infty}^{+\infty}k_x^{-1}K_{1j}e^{-ik_xx}dk_x=\frac{\operatorname{sign}(x)}{2i(k_y^2-k_j^2)}\left(1-e^{-i\sqrt{k_j^2-k_y^2}|x|}\right)$$

$$I_{2j}^{(-1)}=\frac{1}{2\pi}\int_{-\infty}^{+\infty}k_x^{-1}K_{2j}e^{-ik_xx}dk_x=-\frac{1}{2k_j^2}\left(\operatorname{sign}(k_y)e^{-|k_yx|}+i\frac{k_y}{\sqrt{k_j^2-k_y^2}}e^{-i\sqrt{k_j^2-k_y^2}|x|}\right)$$

$$I_{3j}^{(-1)}=\frac{1}{2\pi}\int_{-\infty}^{+\infty}k_x^{-1}K_{3j}e^{-ik_xx}dk_x=-\frac{\operatorname{sign}(x)}{2ik_j^2}\left(e^{-|k_yx|}-e^{-i\sqrt{k_j^2-k_y^2}|x|}\right)$$

$$I_{4j}^{(-1)}=\frac{1}{2\pi}\int_{-\infty}^{+\infty}k_x^{-1}K_{4j}e^{-ik_xx}dk_x=\frac{\operatorname{sign}(x)}{2i}\left\{\frac{1}{k_y^2-k_j^2}+\frac{e^{-|k_y\,x|}}{k_j^2}-\frac{k_y^2}{k_j^2(k_y^2-k_j^2)}e^{-i\sqrt{k_j^2-k_y^2}\,|x|}\right\}$$

$$I_{5j}^{(-1)}=\frac{1}{2\pi}\int_{-\infty}^{+\infty}k_x^{-1}K_{5j}e^{-ik_xx}dk_x=\frac{1}{2\,ik_j\sqrt{k_j^2-k_y^2}}e^{-i\sqrt{k_j^2-k_y^2}\,|x|}$$

$$I_{6j}^{(-1)}=\frac{1}{2\pi}\int_{-\infty}^{+\infty}k_x^{-1}K_{6j}e^{-ik_xx}dk_x=\frac{\operatorname{sign}(x)k_y}{2ik_j(k_y^2-k_j^2)}\left(1-e^{-i\sqrt{k_j^2-k_y^2}\,|x|}\right)$$

Closed form expressions for $I_{ij}^{(0)}\ \left(Im\sqrt{k_j^2-k_y^2}<0\right)$

$$I_{1j}^{(0)}=\frac{1}{2\pi}\int_{-\infty}^{+\infty}K_{1j}e^{-ik_xx}dk_x=\frac{1}{2i\sqrt{k_j^2-k_y^2}}e^{-i|x|\sqrt{k_j^2-k_y^2}}$$

$$I_{2j}^{(0)}=\frac{1}{2\pi}\int_{-\infty}^{+\infty}K_{2j}e^{-ik_xx}dk_x=\frac{k_y}{k_j^2}\frac{\operatorname{sign}(x)}{2i}\left(e^{-i|x|\sqrt{k_j^2-k_y^2}}-e^{-|k_yx|}\right)$$

$$I_{3j}^{(0)}=\frac{1}{2\pi}\int_{-\infty}^{+\infty}K_{3j}e^{-ik_xx}dk_x=\frac{1}{2ik_j^2}\left\{\sqrt{k_j^2-k_y^2}e^{-i|x|\sqrt{k_j^2-k_y^2}}+i|k_y|e^{-|k_yx|}\right\}$$

$$I_{4j}^{(0)}=\frac{1}{2\pi}\int_{-\infty}^{+\infty}K_{4j}e^{-ik_xx}dk_x=\frac{1}{2ik_j^2}\left\{\frac{k_y^2}{\sqrt{k_j^2-k_y^2}}e^{-i|x|\sqrt{k_j^2-k_y^2}}-i|k_y|e^{-|k_yx|}\right\}$$

$$I_{5j}^{(0)}=\frac{1}{2\pi}\int_{-\infty}^{+\infty}K_{5j}e^{-ik_xx}dk_x=\frac{\operatorname{sign}(x)}{2ik_j}e^{-i|x|\sqrt{k_j^2-k_y^2}}$$

$$I_{6j}^{(0)}=\frac{1}{2\pi}\int_{-\infty}^{+\infty}K_{6j}e^{-ik_xx}dk_x=\frac{k_y}{2ik_j\sqrt{k_j^2-k_y^2}}e^{-i|x|\sqrt{k_j^2-k_y^2}}$$

Closed form expressions for $I_{ij}^{(1)}$ $\left(Im\sqrt{k_j^2 - k_y^2} < 0\right)$

$$I_{1j}^{(1)} = \frac{1}{2\pi}\int_{-\infty}^{+\infty} k_x K_{1j} e^{-ik_x x} dk_x = \frac{\mathrm{sign}(x)}{2i} e^{-i|x|\sqrt{k_j^2-k_y^2}}$$

$$I_{2j}^{(1)} = \frac{1}{2\pi}\int_{-\infty}^{+\infty} k_x K_{2j} e^{-ik_x x} dk_x = \frac{k_y}{2ik_j^2}\left(\sqrt{k_j^2 - k_y^2} e^{-i|x|\sqrt{k_j^2-k_y^2}} + i|k_y| e^{-|k_y x|}\right)$$

$$I_{3j}^{(1)} = \frac{1}{2\pi}\int_{-\infty}^{+\infty} k_x K_{3j} e^{-ik_x x} dk_x = \frac{\mathrm{sign}(x)}{2ik_j^2}\left\{\left(k_j^2 - k_y^2\right) e^{-i|x|\sqrt{k_j^2-k_y^2}} + k_y^2 e^{-|k_y x|}\right\}$$

$$I_{4j}^{(1)} = \frac{1}{2\pi}\int_{-\infty}^{+\infty} k_x K_{4j} e^{-ik_x x} dk_x = \frac{\mathrm{sign}(x)}{2ik_j^2}\left\{k_y^2 e^{-i|x|\sqrt{k_j^2-k_y^2}} - k_y^2 e^{-|k_y x|}\right\}$$

$$I_{5j}^{(1)} = \frac{1}{2\pi}\int_{-\infty}^{+\infty} k_x K_{5j} e^{-ik_x x} dk_x = \frac{\sqrt{k_j^2-k_y^2}}{2ik_j} e^{-i|x|\sqrt{k_j^2-k_y^2}}$$

$$I_{6j}^{(1)} = \frac{1}{2\pi}\int_{-\infty}^{+\infty} k_x K_{6j} e^{-ik_x x} dk_x = \frac{\mathrm{sign}(x) k_y}{2ik_j} e^{-i|x|\sqrt{k_j^2-k_y^2}}$$

Closed form expressions for $I_{ij}^{(2)}$ $\left(Im\sqrt{k_j^2 - k_y^2} < 0\right)$

$$I_{1j}^{(2)} = \frac{1}{2\pi}\int_{-\infty}^{+\infty} k_x^2 K_{1j} e^{-ik_x x} dk_x = \frac{\sqrt{k_j^2-k_y^2}}{2i} e^{-i|x|\sqrt{k_j^2-k_y^2}}$$

$$I_{2j}^{(2)} = \frac{1}{2\pi}\int_{-\infty}^{+\infty} k_x^2 K_{2j} e^{-ik_x x} dk_x = \frac{k_y}{k_j^2}\frac{\mathrm{sign}(x)}{2i}\left\{\left(k_j^2 - k_y^2\right) e^{-i|x|\sqrt{k_j^2-k_y^2}} + k_y^2 e^{-|k_y x|}\right\}$$

$$I_{3j}^{(2)} = \frac{1}{2\pi}\int_{-\infty}^{+\infty} k_x^2 K_{3j} e^{-ik_x x} dk_x = \frac{1}{2ik_j^2}\left\{\left(k_j^2 - k_y^2\right)^{3/2} e^{-i|x|\sqrt{k_j^2-k_y^2}} - i|k_y|^3 e^{-|k_y x|}\right\}$$

$$I_{4j}^{(2)} = \frac{1}{2\pi}\int_{-\infty}^{+\infty} k_x^2 K_{4j} e^{-ik_x x} dk_x = \frac{1}{2ik_j^2}\left\{k_y^2\sqrt{k_j^2 - k_y^2} e^{-i|x|\sqrt{k_j^2-k_y^2}} + i|k_y|^3 e^{-|k_y x|}\right\}$$

$$I_{5j}^{(2)} = \frac{1}{2\pi}\int_{-\infty}^{+\infty} k_x^2 K_{5j} e^{-ik_x x} dk_x = \frac{\mathrm{sign}(x)\left(k_j^2-k_y^2\right)}{2ik_j} e^{-i|x|\sqrt{k_j^2-k_y^2}}$$

$$I_{6j}^{(2)} = \frac{1}{2\pi}\int_{-\infty}^{+\infty} k_x^2 K_{6j} e^{-ik_x x} dk_x = \frac{k_y\sqrt{k_j^2-k_y^2}}{2ik_j} e^{-i|x|\sqrt{k_j^2-k_y^2}}$$

Note: $\left(k_j^2 - k_y^2\right)^{3/2}$ must be calculated as $\left(k_j^2 - k_y^2\right)\sqrt{k_j^2 - k_y^2}$, with $Im\sqrt{k_j^2 - k_y^2} < 0$; a direct use of the expression $\left(k_j^2 - k_y^2\right)^{3/2}$ might possibly assign the wrong sign to the result.

Appendix C. Supplementary material

Supplementary data associated with this article can be found, in the online version, at http://dx.doi.org/10.1016/j.compstruc.2015.08.012.These data include MOL files and InChiKeys of the most important compounds described in this article.

References

[1] Alves Costa P, Calçada R, Silva Cardoso A. Vibrations induced by railway traffic: prediction, measurement and mitigation. In: Calçada R, Xia H, editors. Traffic induced environmental vibrations and control: theory and application. Nova; 2013. p. 48–89.

[2] Tadeu A, Antonio J. 2.5 D Green's functions for elastodynamic problems in layered acoustic and elastic formations. Comput Model Eng Sci 2001;2(4):477–96.

[3] Haskell N. The dispersion of surface waves on multilayered media. Bull Seismol Soc Am 1953;43(1):17–43.

[4] Thomson W. Transmission of elastic waves through a stratified solid medium. J Appl Phys 1950;21(0):89–93.

[5] Kausel E, Roësset J. Stiffness matrices for a layered soils. Bull Seismol Soc Am 1981;71(6):1743–61.

[6] Kausel E. Wave propagation in anisotropic layered media. Int J Numer Methods Eng 1986;23(8):1567–78.

[7] Stamos AA, Beskos DE. 3-D seismic response analysis of long lined tunnels in half-space. Soil Dyn Earthq Eng 1996;15(2):111–8.

[8] Sheng X, Jones CJC, Thompson DJ. Modelling ground vibration from railways using wavenumber finite- and boundary-element methods. Proc Roy Soc A: Math Phys Eng Sci 2005;461(2059):2043–70.

[9] François S, Schevenels M, Galvín P, Lombaert G, Degrande G. A 2.5D coupled FE-BE methodology for the dynamic interaction between longitudinally invariant structures and a layered halfspace. Comput Methods Appl Mech Eng 2010;199(23–24):1536–48.

[10] Kausel E, Seale SH. Dynamic and static impedances of cross-anisotropic halfspaces. Soil Dyn Earthq Eng 1990;9(4):172–8.

[11] Barbosa J, Park J, Kausel E. Perfectly matched layers in the thin layer method. Comput Methods Appl Mech Eng 2012;217–220(0):262–74.

[12] Kausel E. Dynamic point sources in laminated media via the thin-layer method. Int J Solids Struct 1999;36(31):4725–42.

[13] Kausel E. Thin layer method: formulation in the time domain. Int J Numer Methods Eng 1994;37(6):927–41.

[14] Barbosa J, Kausel E. The thin-layer method in a cross-anisotropic 3D space. Int J Numer Methods Eng 2012;89(5):537–60.

[15] Kausel E, Peek R. Boundary integral method for stratified soils. Massachusetts Institute of Technology, Department of Civil Engineering; 1982.

[16] Kausel E. Accurate stresses in the thin layer method. Int J Numer Methods Eng 2004;61(3):360–79.

[17] Boas ML. Mathematical methods in the physical sciences. New York: John Wiley & Sons; 1983.

[18] Dominguez J. Boundary elements in dynamics. Southampton: Computational Mechanics Publications; 1993.

[19] Guiggiani M, Gigante A. A general algorithm for multidimensional Cauchy principal value integrals in the boundary element method. J Appl Mech 1990;57(906).

[20] Mantic V. A new formula for the C-matrix in the Somigliana identity. J Elasticity 1993;33(3):191–201.

[21] Kausel E, Barbosa J. PMLs: a direct approach. Int J Numer Methods Eng 2011;90(3):343–52.